C.P. No. 985

C.P. No. 985

MINISTRY OF TECHNOLOGY

AERONAUTICAL RESEARCH COUNCIL

CURRENT PAPERS

Measurements of Pressure Fluctuations and Skin Friction on the Upper Surface of a Slender Wing at Lift (M = 0.8 to 2.0)

by

K. J. Turner and D. Walker

LONDON: HER MAJESTY'S STATIONERY OFFICE

1968

PRICE 10*s* 6*d* NET

U.D.C. No. 533.6.048.2:531.787:532.526.7:533.693.3:533.6.011.35

C.P. No. 985*
October 1966

MEASUREMENTS OF PRESSURE FLUCTUATIONS AND SKIN FRICTION ON THE UPPER SURFACE OF A SLENDER WING AT LIFT (M = 0·8 to 2·0)

by

K. J. Turner

D. Walker

SUMMARY

Four slender-wing free-flight models were used to investigate the local pressure fluctuations, skin-friction and static-pressures across one spanwise station under varying conditions of lift and Mach number. At Mach numbers between 0·8 and 1·2 a well-established free-vortex flow was achieved over the upper surface. The intention was to determine the ratio between the intensity of the pressure fluctuations and the local skin-friction under conditions of attached and separated flows.

While measurements of reasonable quality were obtained, the inherent limitations of the telemetry system did not allow a sufficiently broad band of pressure-fluctuation frequencies to be measured so that the relationship with skin-friction could not be determined. Therefore, a detailed analysis of the results and comparison with other experimental or theoretical data has not been attempted. But the present results are considered to be a useful and significant addition to the rather meagre experimental data that exists on this subject, particularly because they were obtained in conditions free from flow imperfections such as free-stream turbulence which exist in most wind-tunnels.

---

* Replaces R.A.E. Technical Report 66339 - A.R.C. 29059

CONTENTS

1 INTRODUCTION

The existence of pressure fluctuations on the surface of an aircraft or missile may have important repercussions on certain aspects of the design. For example, the fluctuations may manifest themselves as noise in the audio-frequency band and thus require special acoustic insulation for the cabin, or they may excite structural vibrations leading towards fatigue failure of particular components such as skin panels. Such pressure fluctuations may arise from several different types of flow,

(i) turbulence within an attached boundary layer

(ii) an unsteady separated flow

(iii) jet noise.

This paper is mainly concerned with an investigation into the pressure fluctuations under the leading-edge vortices that lie above a slender wing at incidence. In this case there will be pressure fluctuations arising from turbulence velocities within the local boundary layer but the possibility exists that the vortices themselves might have unsteady components that induce additional fluctuating pressure loads on the wing.

Some early low-speed experiments made by Owen[1] in the R.A.E. $11\frac{1}{2}$ ft low-turbulence tunnel had suggested that this was the case and that, immediately under the vortex cores, there was a narrow region where the fluctuating pressures were about three times the amplitude of those expected from the local boundary layer. The present tests were therefore made to investigate the phenomenon at transonic speeds and at supersonic speeds up to $M = 2$.

The experimental investigation of such pressure fluctuations is fraught with difficulties. Firstly because of the instrumentation problems involved in measuring low-amplitude pressure fluctuations over a very wide frequency band and secondly, because of difficulties in analysing and interpreting the experimental data. Wind-tunnel tests raise the additional problem of discriminating between the pressures under investigation and extraneous effects arising from unsteadiness in the main-stream flow. Special wind tunnels[2] have enabled reasonably reliable results to be obtained at subsonic speeds but attempts to use the R.A.E. 8 ft × 8 ft supersonic wind tunnel have been largely unsuccessful because of the spurious signals arising from the background vibration and turbulence. There was, therefore, an obvious advantage to be gained by conducting such experiments on free-flight models. As well as

avoiding the background turbulence problem, free-flight tests can be made at much higher dynamic pressures so that the fluctuating pressures become larger and therefore easier to measure. On the other hand new problems arise from the need to telemeter the measurements.

The present Report describes the tests made on four geometrically identical models of an idealised slender-wing aircraft configuration. These models were originally designed for experiments on dynamic stability and on the second model in the present series stability tests were, in fact, being made simultaneously with the measurements of fluctuating pressure although the results are not discussed here. These attempts on the first two models to measure fluctuating pressures were of an exploratory nature, and were primarily intended to see whether such experiments could successfully be performed in free-flight. Both of these models were instrumented to measure the pressure fluctuations at one point only on the wing surface under the leading-edge vortex. The results were encouraging enough to justify the building of a third model which was equipped to measure the fluctuating pressures at four points along one spanwise line and, simultaneously, the local skin-friction at two of them. The significance of the skin-friction measurements was to establish whether or not the ratio between the rms value of the pressure fluctuations and the local skin friction, that had been observed in some of the subsonic wind-tunnel tests[8], was maintained at supersonic speeds and under the vortex. The results from the third model could not be interpreted properly without some further information on the local flow regimes over the wing surface. A fourth model was therefore made which was instrumented to measure the static pressure distribution along the same spanwise line and also the local flow angle at a point under the vortex corresponding to one of the measuring stations for fluctuating pressure.

When the results from all these four models were collated it was obvious that the original question, does the vortex flow impose additional fluctuating pressures to those arising within the boundary layer, could still not be answered with any confidence. The main limitation of the fluctuating pressure measurements was that the instrumentation system could not handle frequences much above 20 kc/s. The spectrum actually measured is 200 c/s to 20 kc/s and includes only about half the total turbulence energy in the flow.

However, in spite of their limitations, the results from this series of free-flight tests are worth reporting because they represent some of the first measurements obtained of fluctuating pressures under a separated vortex flow

at transonic and supersonic speeds. Furthermore, the experience gained from these tests gives some hope that the free-flight technique can be used to good advantage in work of this kind providing due consideration is given to designing the experiments in such a way that the high-frequency limitations of the telemetry link are less important. This could be achieved, for investigations of attached-flow conditions, by having a boundary layer of much higher Reynolds number.

2 DESCRIPTION OF THE MODELS

All four models were of the same configuration, a general arrangement drawing is given in Fig.1. The wings were of a "sandwich" construction, having a $\frac{1}{4}$ inch thick aluminium-alloy centre plate forming the planform, and hence the leading and trailing edges, with hollow fibre-glass mouldings glued above and below to provide the required thickness and profile. A detachable hatch was fitted in the upper surface to give access to the instrumentation system. (Fig.4.) All the spanwise cross-sections were simple diamonds formed by straight line generators from the centre-line profile to the leading edges. Transition strips, composed of carborundum powder and starting 0·1 inch from the leading edge and 0·5 inch wide, were applied to the upper and lower surfaces along the whole length of the leading edges. On Model 1 the grit size was 0·007 inch but on Models 2, 3 and 4 it was reduced to 0·0035 inch. At the trailing edge two fixed elevators provided the pitching moment for the required trim condition. The two halves of the elevator were set at slightly different angles to produce a rolling moment so that the model performed a slow barrel roll as it flew down the range. This was necessary to ensure that the models did not stray outside the range boundaries. On Model 1 the mean elevator angle was 4·5 degrees, but on the subsequent models it was increased to 10 degrees. Each model was accelerated to its maximum velocity by a single solid-fuel rocket motor which separated at the end of the boosting phase leaving the model in a 'clean configuration' for the coasting part of the flight while the measurements were being taken.

The models were all equipped with R.A.E. sub-miniature 465 Mc/s telemetry systems but the detail arrangements varied considerably from model to model. Because the experiment on Model 1 was of a very preliminary nature it carried only a simple system consisting of one single-channel telemetry set to transmit the fluctuating pressure data from one point on the wing (0·5 C_o, 0·84 s) and one multi-channel set to transmit the information from normal and lateral

accelerometers at the c.g. and a normal accelerometer at the rear. The spanwise station for the fluctuating pressure transducer was chosen to be as nearly under the vortex core, for most of the flight, as could be estimated.

Model 2 was used primarily for an investigation of dynamic stability at lift and carried a multi-channel telemetry set with a complete array of accelerometers to measure all the components of motion and a differential-pressure probe at the nose for determining incidence and sideslip. A single-channel telemetry set was used to transmit the fluctuating pressure information from one point on the wing. Because of the other equipment in the model this pressure transducer had to be mounted further forward on the wing than the transducer in Model 1. It was, however, placed at the same non-dimensional spanwise position 0·84 s (Fig.2). The only aerodynamic difference between the measuring stations on Models 1 and 2 was therefore a small change in Reynolds number and a small difference in local leading-edge angle (24·4 degrees on Model 1 and 26·8 degrees on Model 2).

Model 3 was instrumented entirely for the investigation of pressure fluctuations and local skin-friction. This required a more complicated telemetry system with two multi-channel sets. The geometric arrangement of the pressure transducers and surface-pitot tubes, for the skin-friction measurements[4], is shown in Fig.2. With this arrangement of pressure transducers it was hoped that the inboard one, at 0·5 s would be in an attached flow region (Fig.5) for the whole of the flight and that the re-attachment line of the primary vortex would sweep across the other three as the incidence increased during the flight. A fifth pressure transducer was mounted at 0·6 s in such a way that it was sealed off from any pressure variations on the wing surface. It therefore was sensitive to vibration forces alone and the intention was that, in this way, a qualitative indication would be obtained of the vibration component present in the records from the other four pressure transducers. In addition to the instruments shown, the model carried normal and lateral accelerometers at the c.g. and tail and a differential pressure incidence/yaw probe for determining the trim conditions.

A complete description of the transducers and telemetry systems used for the fluctuating pressure measurements is given in Appendix A.

Model 4 carried one multi-channel telemetry set with normal and lateral accelerometers at the c.g., a lateral accelerometer at the tail, an incidence/yaw probe and 16 pressure transducers. Thirteen of these were used to measure

the static pressure distribution across the upper surface semi-span at the mid-chord (Fig.3) and the other three were connected to surface pitot tubes, arranged as shown in Fig.3. The razor blades at stations 15 and 16 were mounted orthogonally to each other with the intention that the local flow angle could then be resolved from the known variation of surface-pitot pressure with local flow angle[4]. The razor blade at station 14 was mounted at an angle which was estimated to be roughly normal to the local flow under the vortex so that a good measurement of the local skin-friction could be obtained.

3 DISCUSSION OF RESULTS

3.1 Flight conditions

Although the models were geometrically identical and boosted by the same kind of rocket motor there were, of course, differences in their flight conditions. This was mainly because of the different altitudes reached (apogees varying between 2560 ft and 5050 ft), but also because of the lower drag of Model 1 arising from its lower trimmed lift. The time histories of velocity, Mach number, dynamic pressure and Reynolds number are plotted for all the models in Fig.6.

Curves showing the variation of trim lift coefficient and incidence with Mach number are given in Fig.7. The sudden increase in C_L and incidence as the models decelerate though the transonic range is clearly evident and occurs mainly because of the decrease in static margin from the supersonic to the subsonic conditions. The lower trim levels of Model 1 compared with the other three follows from its smaller elevator angle (4·5 degrees compared with 10 degrees). It is evident that Model 4 trimmed at a slightly lower value than Models 2 and 3. This is consistent with its slightly further forward c.g. position.

The general level of incidence and lift coefficient that could be achieved was limited by consideration of flight-path control. At Mach numbers between 2·0 and 1·0 Models 2, 3 and 4 were flying with a normal acceleration of between 7 and 8g. As they decelerated through the transonic region the normal acceleration peaked to about 12g. This was thought to be the limit that could safely be used, in conjunction with the barrel-roll manoeuvre, bearing in mind that the models did not carry any form of self-destruction device that could be operated if they flew beyond the range boundaries.

Wind tunnel tests have shown that, for wings of this configuration, the leading-edge vortex type of flow does not become established until the incidence has reached about 2 degrees. The curves of trim incidence (Fig.7(b)) show that this condition is not reached until the Mach number has fallen to about 1·04 on Model 1 and between 1·4 and 1·2 for Models 2, 3 and 4. At higher Mach numbers, therefore, the pressure fluctuation would be measured in a region of attached flow. But as the vortex flow developed with the simultaneously increasing incidence and falling Mach number the re-attachment line would move across the measuring stations. At the lower Mach numbers therefore some measurements were obtained in the region under the vortex.

3.2 Rms pressures

In Fig.8(a) a comparison is made between the rms pressures measured at approximately the same spanwise position on Models 1, 2 and 3 and Fig.8(b) shows the spanwise variation of rms pressure measured on Model 3. It is important to stress here that these values of rms pressure do not represent the total energy present in the turbulent flow because the instrumentation system could not handle pressures fluctuating at frequencies below 200 c/s and above 20 kc/s. Within the measured frequency band, however, several interesting features can be seen. Very similar results have been obtained from Models 2 and 3 where the trim conditions were similar and the same kind of fluctuating pressure transducers were used. This encourages one to believe that the whole instrumentation and analysis system is giving consistent results. But in the case of Model 1 there is a marked difference below M = 1·2 where the rms pressure falls away with decreasing Mach number before rising very suddenly indeed near sonic speed. Some aspects of this behaviour which are evident from the spectral density distributions are discussed in paragraph 3.5. In the results from Model 3 (Fig.8(b)) of the spanwise distribution of rms pressure, three characteristics stand out.

(1) At Mach numbers below about 1·6 the rms pressures at the inboard station, 0·5 s, are markedly lower than at all the other stations. This immediately suggests that the re-attachment line of the primary vortex lies somewhere between 0·5 s and 0·75 s.

(2) The curve for the transducer at 0·75 s does not follow the general pattern, as it shows particularly high values at the highest and lowest Mach numbers of the test.

(3) The rms pressures measured at stations 0·825 s and 0·9 s increase smoothly as the Mach number falls from M = 1·4 to 1·2 and as the local flow changes from an attached to a free-vortex condition.

The signal from the vibration monitoring transducer is at a very low level throughout the flight, although it increases somewhat as the Mach number falls and the intensity of the pressure fluctuation increases. The vibration amplitude has not been subtracted from the outputs of any of the pressure transducers because it is only a very crude measurement. The curve shown in Fig.8(b) represents an upper limit of the vibration signal recorded and should be used only as a qualitative guide in assessing the pressure measurements from the other transducers. Evidently the results obtained at stations 0·75 s, 0·825 s and 0·9 s at the lower Mach numbers are little affected by any spurious vibration effects. On the other hand it is impossible to obtain a very accurate measure of the low-amplitude pressure fluctuation in the attached-flow region at 0·5 s or at any station at Mach numbers much above 1·6.

3.3 Local flow conditions

A selection of the spanwise static pressure distributions obtained from Model 4 are plotted in Fig.9. The rapid development of the vortex at Mach numbers below 1·3, corresponding to incidences above 2 degrees, can be inferred from the rapidly increasing suctions at the outboard stations. The local peaks in the pressure distributions at 0·72 s are somewhat surprising. They do not seem to have been apparent in any other experiments and it is difficult to find a theoretical explanation for them. The experimental records outboard of 0·8 s are similar to those observed in wind-tunnel tests on slender wings[5]. In the present results the peaks at about 0·72 s seem firmly anchored to the same spanwise position in spite of the clear development of the vortex flow. It does not seem likely that this is a spurious result arising from the malfunction of one pressure transducer since the shape of the pressure distribution curves in this region are defined by two or three pressure measurements.

Turning to the measurement of the local flow direction (Fig.10) it is evident that the vortex flow sweeps across the station at 0·825 s at about M = 1·2, corresponding to an incidence of 2 degrees. But the very large local flow angle of more than 70 degrees which is indicated at incidences above 3 degrees is most unlikely. In deriving this flow angle the original intention of resolving the measurements from the two orthogonal surface-pitot tubes 15 and 16 (Fig.3) could not be realised because the transducer at

station 15 did not work properly. The resolution was therefore attempted using the measurements from the surface pitot-tube facing the free/stream direction (No.16) on the starboard wing and the tube angled at 41·5 degrees (No.14) on the port wing. This assumes, of course, that the flow is perfectly symmetrical on both sides of the wing. Further errors must certainly arise because these two measuring stations are not at precisely the same spanwise location. But the main source of error must lie in the assumption that the local surface pressure varies with $\cos^2 \theta$. This relationship has been verified for local flow angles up to 30 degrees[4] and might be extrapolated up to, say 40 degrees. But it is certainly unjustifiable for angles as great as the 70 degrees indicated relative to the pitot-tube at station 16. On the basis of oil-flow studies made on a similar wing under similar conditions in a wind-tunnel[6] a more likely curve has been plotted in Fig.10. Here an assumption is made that the present measurement of the incidence and Mach number at which the local flow starts to swing round is correct although the magnitude of the turning angle is wrong. A maximum flow angle, $\theta = 45^\circ$ has therefore been assumed, on the basis of wind-tunnel evidence, and the smaller angles have been reduced in proportion.

3.4 Relationship between local skin-friction and rms pressure*

The local skin-friction coefficients, derived from the measurements obtained from the surface-pitot tubes, on Models 3 and 4 are plotted in Fig.11. The dotted portions of the curves between M = 0·95 and 1·4 are interpolations to cover the region within which no adequate calibration equations exist relating the skin friction to the surface-pitot pressure.

On the basis of the flow direction data of Fig.10 the skin-friction component in the free-stream direction (Fig.11(a)) is, of course, the skin friction for stations 0·5 s at all Mach numbers and 0·825 s, at Mach numbers above 1·3. At Mach numbers below 1·3 the local flow persists in the free-stream direction at station 0·5 s but swings round through above 40 degrees at station 0·825 s. The fact that the free-stream skin-friction values for these two points are coincident at M = 0·95 and 0·8 is probably mere chance. When due allowance is made for the local flow angle at station 0·825 s the skin-friction is, of course, much higher than for the inboard station (Fig.11(b)).

It is possible to compare the measured skin-friction with estimated values for the condition where the flow is attached since the boundary-layer

* Rough estimates of the local skin-friction are made and presented in this section. An attempt is made to compare them with the rms pressure as it was thought[8] at the time the analysis was done that there was a correlation between them. Recent unpublished work by Owen indicates that there would not be such a correlation, at any rate in the frequency range within which the measurements were taken.

run can be defined. The estimated curve (Fig.11(a)) has been taken from Ref.7 where calculations were made for an identical free-flight model. But under the vortex no attempt has been made to estimate the skin-friction since boundary-layer conditions are so complicated and the appropriate boundary-layer run is not known. Working backwards, however, from the measured values of skin-friction (in the local-flow direction) the theoretical boundary-layer run would be about one inch. This is roughly the distance along a streamline from the re-attachment line to the measuring station at 0·825 s which suggests that the boundary-layer probably starts afresh at the re-attachment line with little entrainment of the thicker boundary-layer flow from the inboard region.

The ratio between the local rms pressure and skin-friction is of considerable interest. Theoretical and experimental studies have indicated that this ratio is about two for conditions under a two-dimensional attached boundary-layer. Wyatt and Owen[8] have tentatively shown, from their low-speed wind-tunnel tests, that the ratio is maintained under the vortex. This suggests that all the increase in fluctuating pressure under the vortex arises from the high-shear boundary-layer conditions there and that there is no additional component introduced from any unsteadiness in the vortex flow itself. In the present tests it was hoped that a similar line of reasoning could be pursued to see if this condition still held in supersonic flow.

In Fig.12 the ratio of the local rms pressure to the local skin friction is plotted, from the combined results of Models 3 and 4, for the inboard station (0·5 s) in the region of attached flow and for one of the outboard stations (0·825 s) under the vortex. The result for the inboard station, where one might expect the ratio to be about 2, is clearly very low. The amount that the curve falls below $\sqrt{\overline{p^2}}/\tau = 2$ is probably indicative of the energy in the turbulence spectrum above 20 kc/s that has not been measured. Bearing in mind the limited frequency range, the high level of the curve of the outboard station is somewhat surprising. One would expect that the thinner boundary-layer in this region would have a larger proportion of its turbulent energy at the higher frequencies outside the measured band and therefore not included in the rms value. Does the 'measured' ratio $\sqrt{\overline{p^2}}/\tau \simeq 2$ under the fully developed vortex flow below M = 1·3 therefore imply that there is a considerable degree of turbulence being added by the vortex flow? Unfortunately the uncertainties in the measurements of rms pressure (because of the frequency limitation) and in the measurements of skin-friction (because of uncertainty in the local flow angle) makes this question impossible to answer from the present tests.

3.5 Spectral density distributions

A small sample of all the spectral density distributions of $(\text{pressure})^2$ obtained, is given in Figs.13 and 14. Comparisons are made in Fig.13 between the distribution at the (nearly) common station 0·84 s and 0·825 s on Models 1, 2 and 3 while Fig.14 shows the spanwise variations obtained on Model 3.

On comparing the results between the three models, at the transonic Mach number 0·97, there is little difference in the shapes of the distributions, apart from a small peak at 2300 c/s on Model 1 although there is considerably more energy present in Model 1 than in the other two as has already been noted. But at $M \simeq 1{\cdot}2$ the distribution from Model 1 is seen to be markedly different from the others with a large part of the energy concentrated in the band 3000 to 8000 c/s. This 'peaky' distribution was evident on Model 1 at all supersonic speeds although the peak collapsed quite suddenly transonically. Peaks of this magnitude did not appear in any of the spectral density distributions from the other two models and they therefore probably represent a spurious result from the early and inferior type of pressure transducer used on Model 1.

Bearing in mind the difficulties of the experimental technique, the degree of similarity between the results from Models 2 and 3 is gratifying and gives some grounds for confidence that repeatable and meaningful results were being obtained on the later models. Turning now to the more detailed results from Model 3 the subsonic set of curves (Fig.14(a)) show that a rather different spectral shape obtains in the region of attached flow ($y/s = 0{\cdot}5$) compared with the outboard stations under the vortex. At this Mach number the incidence is between 5 and 6 degrees and so a strong vortex has been established over the region covered by the three outermost transducers. It is evident that the middle part of the measured spectrum has been 'filled in' at these stations compared with the inboard one. This is rather surprising when we consider that the very high-shear flow under the vortex would be expected to have a larger part of its energy at the higher frequencies. This 'filling-in' process can be traced through from the results, at higher Mach numbers and lower incidences (Figs.14(b & c)). In fact, apart from the result for station 0·825 s, the trends of the curves have changed completely between $M = 0{\cdot}9$, $\alpha = 6°$ and $M = 1{\cdot}8$, $\alpha = 1{\cdot}5°$. When the spectra are plotted in a non-dimensional form (Figs.15 and 16) these trends are not so evident but the non-dimensional spectra have been given to facilitate comparison with results from other tests. In these plots the frequency has been non-dimensionalised by multiplying by the ratio, local semi-span over velocity, and the spectra function,

$$n\,F(n) \;=\; \text{spectral density} \times \text{frequency} \times \frac{1}{q^2}\,.$$

3.6 Limitation of the instrumentation system

The reliability of the measurement of rms pressure and spectral density from the piezoelectric transducer signals depends on having a high enough signal/noise ratio at the output of the post-discriminator filter (Fig.23(c)). Some indication of this can be obtained by inspection of the 35 mm film record to see whether the isolating channels are clean, as indicated by Fig.20. However, this film was recorded with the normal low pass filter with approximately 3000 c/s cut off, and the effect of increasing this to 20000 c/s must be considered. In an F.M. system, a frequency to voltage discriminator improves the signal to noise power ratio by an amount given by

$$\left(\frac{S}{N}\right)_{out} = \left(\frac{S}{N}\right)_{in} \frac{3}{2} \frac{f_D^2}{f_M^3} f_B$$

where f_D = maximum frequency deviation

f_M = bandwidth of the post-discriminator filter

f_B = bandwidth of the pre-discriminator filter.

This improvement takes place above the discriminator threshold which occurs at an input signal-to-noise power ratio of approximately 12·6:1, and below this level the output signal to noise ratio decreases very rapidly. If we now take the following values of

f_D = 15 kc/s

f_B = 70 kc/s (120 kc/s to 190 kc/s)

f_M = 3 kc/s standard filter

or f_M = 20 kc/s special filter

We find an improvement in signal to noise power of 870 for the 3 kc/s filter, and 2·95 for the 20 kc/s filter. Thus, in the case of the 20 kc/s filter the output signal-to-noise power ratio at threshold will be 37:1. Since the noise voltage output from the discriminator is proportional to frequency, this means that, with a constant spectral density signal from the transducer, the

signal to noise spectral density ratio at the highest frequency, i.e. 20 kc/s would be 12·3:1 and at 10 kc/s the signal to noise spectral density ratio would be 49:1. Thus at threshold we could have an error of approximately 2·7% in total rms pressure measurement, and an error of 8% in spectral density pressure measurement at 20 kc/s. For signals 10db above threshold these errors would be reduced to 0·3% for the rms measurement, and 0·8% for the spectral density. The received R.F. signal strength with respect to threshold is shown in Fig.21 for the two transmitters of Model 3. It is seen that transmitter 2 remained at a level of more than 30db above threshold until 35 sec after launch, whereas transmitter 1 fell below threshold at a time of 18·6 sec and intermittently after this. As a check on the noise-amplitude calculations, samples were analysed from each transmitter on the launcher (i.e. with no transducer signal input) and also a series of samples from the earthed isolating channels from transmitter 1 were joined together and analysed as one sample. These covered the time period 20·6 - 26 sec, but periods when receiver noise was obviously present, e.g. 23·5 sec, were avoided. The resulting equivalent spectral density levels are shown in Fig.22. The mean level from the transducer at 0·825 s on the launcher, Fig.22(a), is seen to be approximately 2×10^{-8} $(psi)^2$/cps. When compared with the white noise calibration of $8{\cdot}8 \times 10^{-6}$ $(psi)^2$/cps, this gives a signal to noise ratio of some 400. This limit could be set in the cathode follower and amplifier stage in the model, or in the recording and replay equipment used on the ground. The background noise between 20·6 and 26 sec on transmitter 1 is shown in Fig.22(b) and is approximately 3×10^{-7} $(psi)^2$/cps at 20 kc/s. The R.F. signal strength at this time was smaller than that for most of the other samples from the transducer at station 0·75 s. If we take the measured spectral densities from this transducer at 20 kc/s as a comparison we have:-

	Transducer at 0·75 s					Background noise
Sample Time sec	4·05-4·55	8·53-8·98	13·98-14·42	16·07-16·52	17·19-17·65	20·6-26
Spect. density at 20 kc/s	$2{\cdot}2 \times 10^{-6}$	2×10^{-6}	$2{\cdot}2 \times 10^{-6}$	$7{\cdot}0 \times 10^{-6}$	$1{\cdot}6 \times 10^{-5}$	$3{\cdot}0 \times 10^{-7}$
*Signal/noise at 20 kc/s	7·3	6·7	7·3	23	53	-

* This assumes that the R.F. signal strength was equal to that of the sample for background noise.

For all the samples shown, the signal level was higher than that at the time of the background noise sample so that the above figures are pessimistic.

If the white noise calibration level of $8{\cdot}8 \times 10^{-6}$ $(psi)^2$/cps is taken as the full scale signal, then the calculated threshold signal to noise ratio of 12·3:1 at 20 kc/s gives a noise spectral density of $7{\cdot}2 \times 10^{-7}$ $(psi)^2$/cps at threshold. This agrees well with the measured background noise spectral density of $3{\cdot}0 \times 10^{-7}$ $(psi)^2$/cps at approximately 3db above threshold.

Using the figure of 12·3:1 signal to noise ratio at threshold, and taking account of the signal strength level with respect to threshold and the magnitude of the transducer output, the following estimate has been made of the errors for the transducer at 0·75 s at 20 kc/s.

Sample time sec	4·05-4·55	8·53-8·98	13·9-14·42	16·07-16·52	17·19-17·65
Spectral density at 20 kc/s	$2{\cdot}2 \times 10^{-6}$	$2{\cdot}0 \times 10^{-6}$	$2{\cdot}2 \times 10^{-6}$	$7{\cdot}0 \times 10^{-6}$	$1{\cdot}6 \times 10^{-5}$
% of * full scale	25	23	25	80	180
db above threshold	16	10	8	3	8
Estimated signal/noise at 20 kc/s	125	28	19	20	140
% error in spec. dens. at 20 kc/s	0·8	3·5	5·1	5·0	0·7

* full scale taken as white noise calibration level.

In the case of transmitter 2, the R.F. signal strength was more than 30db above threshold for all the samples, i.e. for the transducers at 0·825 s and 0·9 s throughout the flight. In this case the signal strength conditions would virtually be the same as on the launcher, and the limits would again be set by the cathode follower and amplifier or by the ground recording and replay equipment.

4 POSSIBILITIES FOR FUTURE WORK

The practicability of using free-flight model for investigations of boundary-layer pressure fluctuations has been clearly demonstrated with this series of models. There is a real advantage in not having any spurious effects from wind-tunnel turbulence superimposed on the boundary-layer turbulence. But the full potential of the technique cannot be realised unless a much more complete spectrum of the turbulence energy can be recorded for analysis. The two avenues towards improvement in this direction are,

(a) to fly models which have a much thicker boundary-layer and hence lower turbulence frequencies,

(b) to improve the operating characteristics of the telemetry and recording system so that higher frequencies can be measured.

These two possibilities will now be examined in turn.

4.1 Aerodynamic considerations

If we postulate that, say 85% of the total turbulence energy must lie within the frequency range 200 - 20000 c/s we may calculate the boundary-layer thickness appropriate to this spectrum and hence the boundary-layer run required. Such calculations based on a rough estimate of the spectrum show that for free-stream velocity of 2000 ft/sec, a boundary-layer run of about 14 ft would be adequate. This would be very easy to achieve for the attached-flow along a simple free-flight model such as an ogive-cylinder but it is probably impossible to achieve, on any reasonably-sized model, for the portion of the boundary-layer under a separated vortex.

It would therefore seem sensible to tackle, at least, the simple attached-flow type of boundary-layer experiment in free-flight. The model could merely be an ogive cylinder about 20 ft long and, say 2 ft diameter housing an internal, non-separating rocket motor. Fluctuating-pressure and skin-friction transducers could be spaced at intervals along the length of the body if simultaneous measurements at different Reynolds numbers were required. One problem might be the excitation of sizeable body vibrations from the separated turbulent base-flow: the base would have to be blunt, to accommodate the rocket-motor nozzle whereas, with the present series of delta wings, a clean trailing-edge separation was assured. If this problem should materialise some improvement could probably be made by changing the type of base-separation to a multicycle vortex type by suitably shaping the after-body.

4.2 Instrumentation considerations

The upper frequency limit of the present technique is set by the frequency of the sub-carrier and the method of recording. Thus if we set a limit of 5 kc/s between the highest signal or modulation frequency, and the lowest of the frequencies of the modulated carrier (this determines the sharpness of the cut off of the post discriminator filter), we have approximately

$$F = (f_M + 5) + 2(f_D + f_M)$$

where F = max. frequency which can be recorded

f_M = max. signal frequency

f_D = frequency deviation.

For

$$F = 100 \text{ kc/s}$$

we have for

$f_D = 5$ kc/s, $f_M = 28$ kc/s $f_B = 2(f_D + f_M) = 66$ kc/s, $\frac{f_D^2 f_B}{f_M^3} = 0{\cdot}075$

$f_D = 10$ kc/s, $f_M = 25$ kc/s $f_B = 2(f_D + f_M) = 70$ kc/s, $\frac{f_D^2 f_B}{f_M^3} = 0{\cdot}45$

$f_D = 15$ kc/s, $f_M = 22$ kc/s $f_B = 2(f_D + f_M) = 74$ kc/s, $\frac{f_D^2 f_B}{f_M^3} = 1{\cdot}5.$

The values used in practice were

$$f_D = 15 \text{ kc/s} \quad f_M = 20 \text{ kc/s} \quad f_B = 70 \text{ kc/s} \quad \frac{f_D^2 f_B}{f_M^3} = 1{\cdot}98$$

Thus by accepting a worse signal to noise ratio at threshold it would be possible to extend the upper frequency limit to 28 kc/s with the present tape recording equipment.

Several alternatives are possible if it is required to extend the upper frequency limit of the tests still further. The same signal to noise improvement at threshold could be maintained by increasing all three frequencies

f_D, f_B and f_M in the same ratio, but the pre-discriminator signal to noise will be proportional to $1/f_B$, i.e. threshold will take place at a larger R.F. signal input. Modifications will be needed to the pre and post discriminator filters, and a higher frequency tape recorder will be required. (Alternatively for the wider bandwidth system, the recording could be made after the frequency/voltage discriminator in real time, when the present recorder would enable frequencies up to 100 kc/s to be recorded.) For higher frequencies still, there is the possibility of using the S.R.D.E. or 450 type telemetry in its single channel form, together with a video tape recorder. The airborne equipment for this is much larger than for the 465 system, and video tape is only available at Woomera. (Increased transmitter power would also be necessary.)

The other approach of choosing a thicker boundary layer has the disadvantage that the magnitude of pressure fluctuation will also be lower and the limiting factor would be the noise of the amplifier first stage. A rough assessment of the amplifier noise can be given by assuming that the noise generating resistor is the 2 MΩ in the grid and the cathode follower, then

$$E^2 = 4\,k\,TRB$$

where E = noise voltage, k = Boltzmann's constant, T = absolute temperature, R = resistance and B = bandwidth. Assuming B = 20 kc/s, this gives

$$E = 18\ \mu V .$$

If the noise figure of the first valve is 6db, then the total noise voltage will be 36 μV. Thus for a S/N ratio of 100:1, the lowest signal voltage which could be measured would be 3·6 mV. This compares with the present level of 125 mV for full scale in Model 3. Estimates show that a 2:1 reduction in rms pressure would be consistent with the increased boundary layer run suggested in Section 4.1, and hence amplifier noise should not be a problem.

5 CONCLUSIONS

Measurements were obtained of the pressure fluctuations under regions of attached and separated-vortex types of flow over the Mach number range 0·8 to 1·8. But the limitations of the instrumentation system precluded

measurements at frequencies above 20 kc/s where much of the turbulence energy lies. This limitation did not allow any meaningful comparison with measurements of the local skin-friction coefficients to be made and so the main purpose of the tests could not be realised.

It would be well worth-while, however, continuing investigations of this type in free-flight if the work is limited to measurements at high boundary-layer Reynolds numbers. It should be possible to do this for attached flows on simple non-lifting bodies of revolution.

Appendix A

INSTRUMENTATION FOR MEASURING FLUCTUATING PRESSURES

A.1 Requirements

The instrumentation requirements were based on the low-speed measurments obtained by Owen in the R.A.E. 11½ ft low turbulence tunnel. These indicated that the magnitude of the pressure fluctuation would be about 0·5 psi rms and the peak pressures would occur in the frequency range 10 kc/s to 20 kc/s depending on Mach number. Ground equipment considerations as discussed later, set the upper limit of frequency measurement at 20 kc/s and a lower limit of 100 c/s to 200 c/s was chosen.

A.2 Transducers

The transducers used in the models were circular disc piezoelectric bimorphs[9]. The one used in Model 1 was rim-clamped and subsequent transducers were all centre supported (Fig.17). Their electrical characteristics were as follows.

Model	Location	Capacity μμF	Natural frequency kc/s	Sensitivity V/psi	Diameter inches
1	0·84 s	1000	45	0·31	0·25
2	0·84 s	140	80	0·152	0·125
3	0·5 s	168	88	0·43	0·125
3	0·75 s	157	100	0·095	0·125
3	0·825 s	180	100	0·225	0·125
3	0·9 s	168	100	0·28	0·125
3	0·6 s	167	87	0·33	0·125

It can be seen that the rim-clamped transducer in Model 1 had a larger diameter, higher capacity, and a lower natural frequency than the remaining transducers. The sensitivity to strain transmitted through the body is less in the case of the centre supported discs, as also is the temperature sensitivity, due to the comparative isolation of the piezoelectric element

from the body. The transducers were calibrated in a small shock-tube by applying a known step-pressure change to them. The pressure equivalent to 1g acceleration normal to the plane of the plate is $5{\cdot}3 \times 10^{-3}$ lb/in^2, for both types of transducer.

A.3 Cathode follower, amplifier and filter

The expected pressure fluctuation level was approximately 0·5 lb/in^2 rms and since the voltage input needed by the telemetry system was 2·5 volts, an amplification of 8 was selected for the first model. The amplification used for subsequent transducers was based on the results obtained from Model 1, and on the position of the transducer in the model. The input impedance of the amplifiers was determined by the capacity of the individual transducer, and by the lowest-frequency pressure fluctuation to be measured. Thus in the case of the centre-supported transducers, an input impedance of 10 MΩ gave a reduction in gain of $\frac{1}{2}$ at 100 c/s compared with that at 1000 c/s. A cathode follower of 10 MΩ input impedance was used for all the transducers, but the low-frequency response was deliberately degraded in Model 1, by feeding through a 100 μμF capacitor, so as to give a quick recovery time. The cathode followers also had to handle, without overloading, any large outputs from the transducers due to "ringing" of the crystal at its natural frequency. Although the ringing frequency would be well above the recording range of the rest of the equipment, distortion in the cathode follower could give rise to spurious frequencies caused by the "envelope" of the ringing. The cathode followers were in fact capable of handling inputs of 20V peak-to-peak without distortion. Low-pass filters were designed to go between the cathode follower and amplifier stages so as to pass frequencies up to 20 kc/s and cut-off the crystal natural frequency, again to avoid distortion due to over-loading in the amplifier stage. M - derived filters were used with damping resistors to remove transient effects. The complete circuits for the cathode follower, filter and amplifier stage for Model 1 are shown in Fig.18. In the subsequent models, the filter cut-off frequency and amplifier gain were adjusted to suit the particular transducer and the expected pressure input.

A.4 Switching arrangement in Model 3

The switching arrangement for Model 3 is shown in Fig.19. The minimum duration of the sample was determined at 0·5 sec by the low-frequency limit of the pressure fluctuations and by the SPADA equipment used for the analysis[10]. Each transducer was connected to its own cathode follower, filter and

amplifier, and the amplifier outputs were sampled at approximately 1 sec intervals. The information from the transducers at stations 0·5 s and 0·75 s was relayed by transmitter No.1, and from the transducers at 0·825 s and 0·9 s by transmitter No.2. Isolating channels were interposed between the transducers for identification purposes. One of these was earthed, and the other was connected to the output of a 24-channel high-speed switch (80 c/s). Thus it was possible to monitor accelerations and skin-friction pressure measurements for periods of 1/12 sec at intervals of 1 sec on each transmitter in turn. The 'dummy' pressure transducer at 0·6 s was also sampled by the high-speed switch. Since however the sampling time was only 1/200 sec, a full spectral analysis was not possible but an approximate rms value could be determined. A qualitative assessment of the vibration amplitudes experienced by the four active pressure transducers could be made by comparison with the dummy one (Fig.20).

Appendix B

GROUND RECORDING SYSTEM

At the ground recording station the telemetry signal was passed through a frequency/voltage discriminator and a low-pass filter before being recorded on film and tape. A short sample of the film record from Model 3 is shown in Fig.20. The film speed was 96 inches/sec and the records from the four piezoelectric transducers and isolating channels can be seen. This record was used for the analysis of data transmitted via the high-speed switch, i.e. accelerations, incidence and yaw measurements, skin-friction, and also for the piezoelectric transducer used for vibration monitoring. The film record was also used as an indication of the reliability of the output from the piezoelectric pressure transducers. The record reproduced in Fig.20(b) shows that transmitter No.2 was working satisfactorily, but that the signal from transmitter No.1 was being masked by receiver noise. The nature of a signal containing receiver noise is seen to be noticeably different from a genuine transducer output. This sample was recorded at 19 seconds, ($M = 0{\cdot}9$), when the signal strength from transmitter No.1 first dropped below the receiver threshold (Fig.21(a)).

The final input required for SPADA is $\frac{1}{4}$ inch amplitude-modulated magnetic tape, and the frequency range of analysis is 10 c/s to 10 kc/s. The Aberporth range recording facilities include $\frac{1}{2}$ inch magnetic tape at a standard speed of 60 inches/sec. The normal airborne sub-carrier is frequency-modulated by the signal output at a mean frequency of 145 kc/s and with a frequency deviation of ±15 kc/s. This frequency is translated after reception, to 50 kc/s ±15 kc/s, and recorded on the $\frac{1}{2}$ inch tape at 60 inches/sec.*

By replaying the $\frac{1}{2}$ inch tape at 30 inches/sec through a frequency/voltage discriminator followed by a low pass filter with 10 kc/s cut-off, the frequencies of the original pressure fluctuations were divided by 2 and recorded on $\frac{1}{4}$ inch tape for SPADA analysis. Pressure fluctuation frequencies up to 20 kc/s were thus recorded as frequencies up to 10 kc/s, and 0·5 sec of flight time became 1·0 sec of SPADA tape time. A block diagram of the complete system is shown in Fig.23.

---

* A synchronisation frequency at 186 kc/s is usually used with this telemetry system and to accommodate this, the telemetry bandwidth is 120-190 kc/s. In order to make maximum use of this available bandwidth, the mean frequency was set to 155 kc/s and the frequency deviation kept at 15 kc/s to allow for the 20 kc/s modulation frequency.

Appendix C

ANALYSIS TECHNIQUE FOR FLUCTUATING PRESSURES

The analysis of the piezoelectric transducer outputs was done by means of SPADA [10]. (Spectral Density and Amplitude Distribution Analyser.) This analyser covers the frequency range 10 c/s - 10 kc/s, but because of the recording technique described in Appendix B this corresponds to 20 c/s - 20 kc/s for the transducer frequencies. The signal to be analysed is recorded on $\frac{1}{4}$ inch magnetic tape at 16 cm/sec and is replayed at a speed which varies continuously from 160 cm/sec to 16 cm/sec through three fixed frequency filters with centre frequencies at 100 c/s, 1000 c/s and 10000 c/s and relative bandwidths $\left(\delta = \frac{\Delta f}{f}\right)$ of 0·25, 0·12 and 0·58 respectively. A 15 second sample is the longest one which can be analysed and shorter samples are made up to the same length tape loop by the addition of blank tape. A sampling error is introduced if the sample time is too short and a minimum time of 0·5 sec of flight time i.e. 1·0 sec of analyser time was used. The spectral density of the signal is obtained in the form

$$\left[\overline{\sigma^2}\right]_{f_1}^{f_2} = \frac{\left[(y\ \mathrm{rms})^2\right]_{f_1,t_1}^{f_2,t_2}}{\Delta f}$$

where $\left[y(t)\right]_{f_1,t_1}^{f_2,t_2}$ denotes the vibration time function recorded over the period $t_1 - t_2$ in the frequency range $f_1 - f_2$ and $\overline{\sigma^2}$ is the average value of the spectral density within these limits. The analyser produces a plot of the spectral density of the signal against frequency, and this is compared with a similar plot for the spectral density of a white noise source of known amplitude recorded through the same complete system. A Dawe instruments white noise generator with 20 kc/s cut-off was used, and this was connected to the cathode follower input instead of each piezoelectric transducer in turn. The resulting signal was recorded shortly before firing in the same way as the flight record. Because of the shape of the cut-off of the filter in the white noise generator, the spectral density of the source was not constant up to 20 kc/s. A correction therefore had to be applied to the spectral density distribution obtained from each of the pressure transducers to allow for this effect.

SYMBOLS

C_o	centre line chord
s	semi span
C_L	lift coefficient
M	Mach number
τ	skin friction
α	angle of incidence
n F(n)	spectral density × frequency × $\frac{1}{q^2}$
q	dynamic pressure
f_D	maximum frequency deviation
f_M	bandwidth of post discriminator filter
f_B	bandwidth of pre-discriminator filter
F	maximum frequency of tape recorder
k	Boltzmann's constant
$\overline{\sigma^2}$	average value of spectral density

REFERENCES

No.	Author	Title, etc.
1	T.B. Owen	Unpublished Mintech Report.
2	A.L. Kistler W.S. Chen	The fluctuating pressure field in a supersonic turbulent boundary layer. P107458 U.S.A. California Inst. Tech. JPL Report 32-277 1962-08
3	K.J. Turner A.J. Ross G. Earley	The dynamic stability derivatives of a slender wing. A comparison of theory with free-flight model tests at near-zero lift, M = 0.8 to 2.4. R.A.E. Tech. Report No.66170, June 1966 A.R.C. 28574
4	K.G. Smith L. Gaudet K.G. Winter	The use of surface pitot tubes as skin-friction meters at supersonic speeds. A.R.C. R & M 3351, June 1962
5	J.W. Britton	Pressure measurements at supersonic speeds on three uncambered conical wings of unit aspect ratio. A.R.C. C.P. 641, May 1962
6	L.C. Squire	The characteristics of some slender cambered gothic wings at Mach numbers from 0.4 to 2.0. A.R.C. R & M No.3370, May 1962
7	J.B.W. Edwards	Measurements of skin-friction using surface pitot tubes in free flight at supersonic speeds. A.R.C. C.P. 711, April 1963
8	L.A. Wyatt T.B. Owen	Preliminary low speed measurements of skin-friction and surface pressure-fluctuations on a slender wing at incidence. R.A.E. Tech. Note Aero No.2916 (A.R.C. 25436) September 1963
9	W.R. Macdonald P.W. Cole	New piezoelectric pressure transducers for aerodynamic research. R.A.E. Tech. Note I.R. No.23, April 1963 A.R.C. 25056
10	S.L. Entres	The analysis of complex vibrations with SPADA. A.R.C. C.P. 570, June 1960

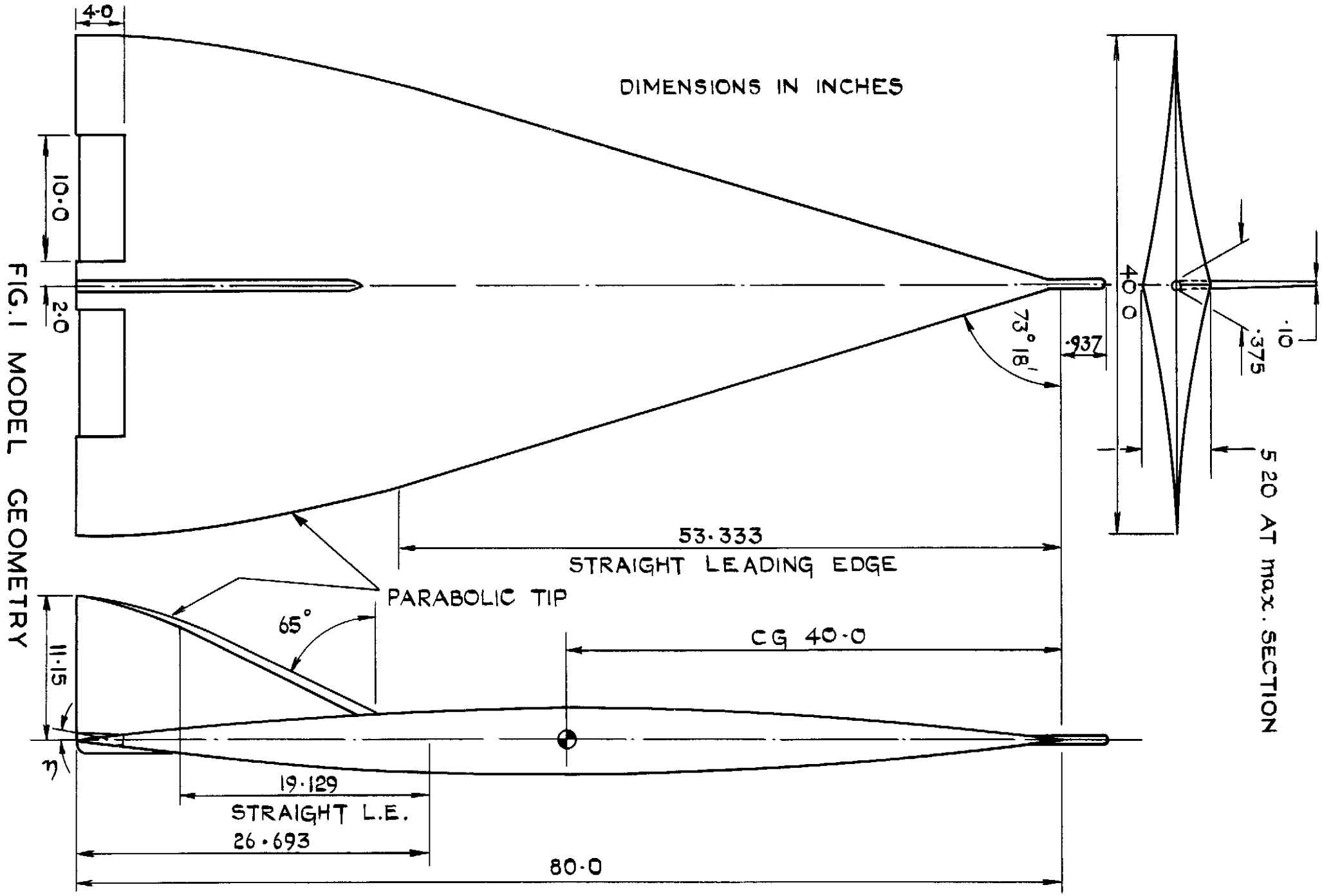

FIG. 1 MODEL GEOMETRY

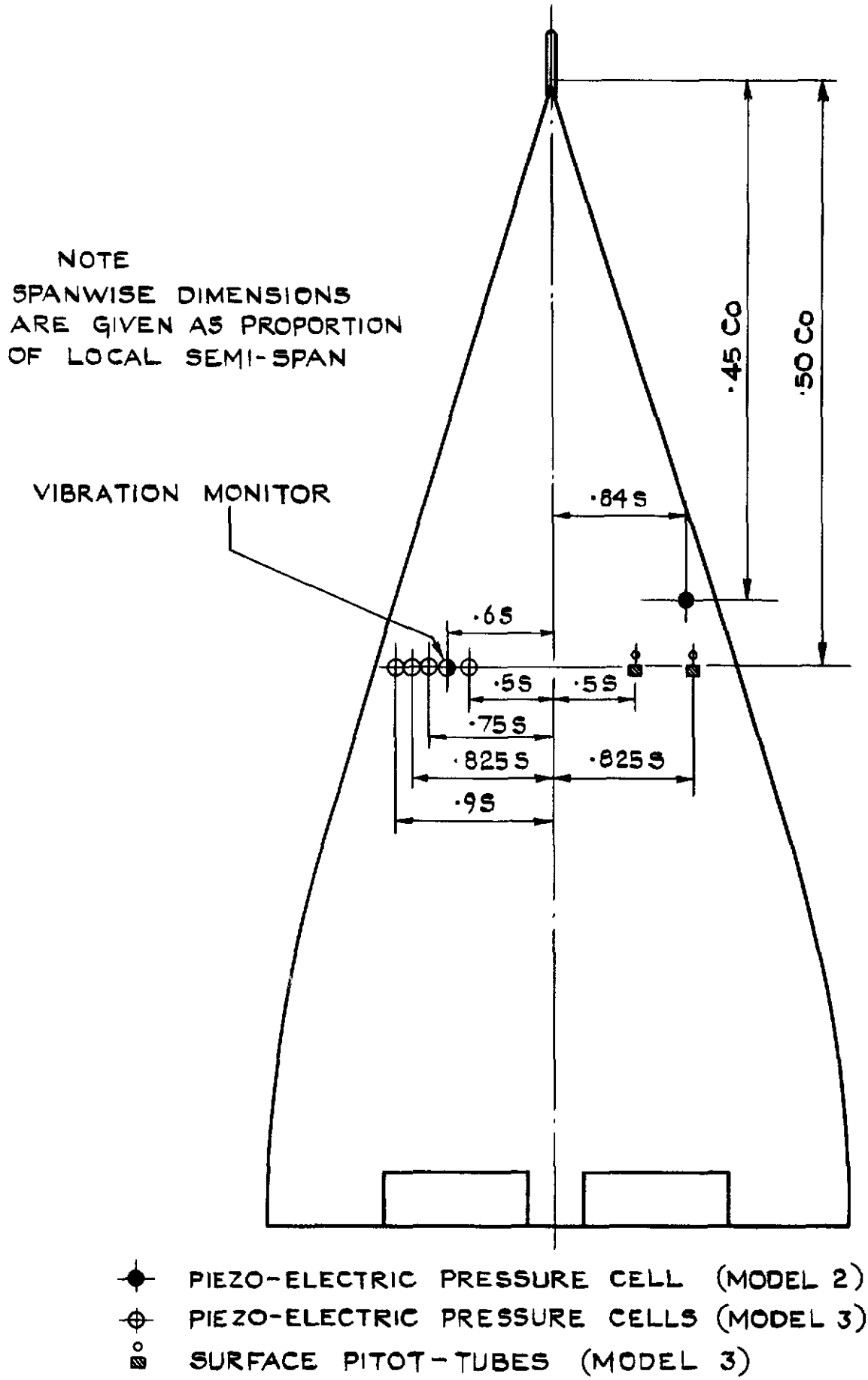

FIG. 2 INSTRUMENT POSITIONS (MODELS 2 & 3)

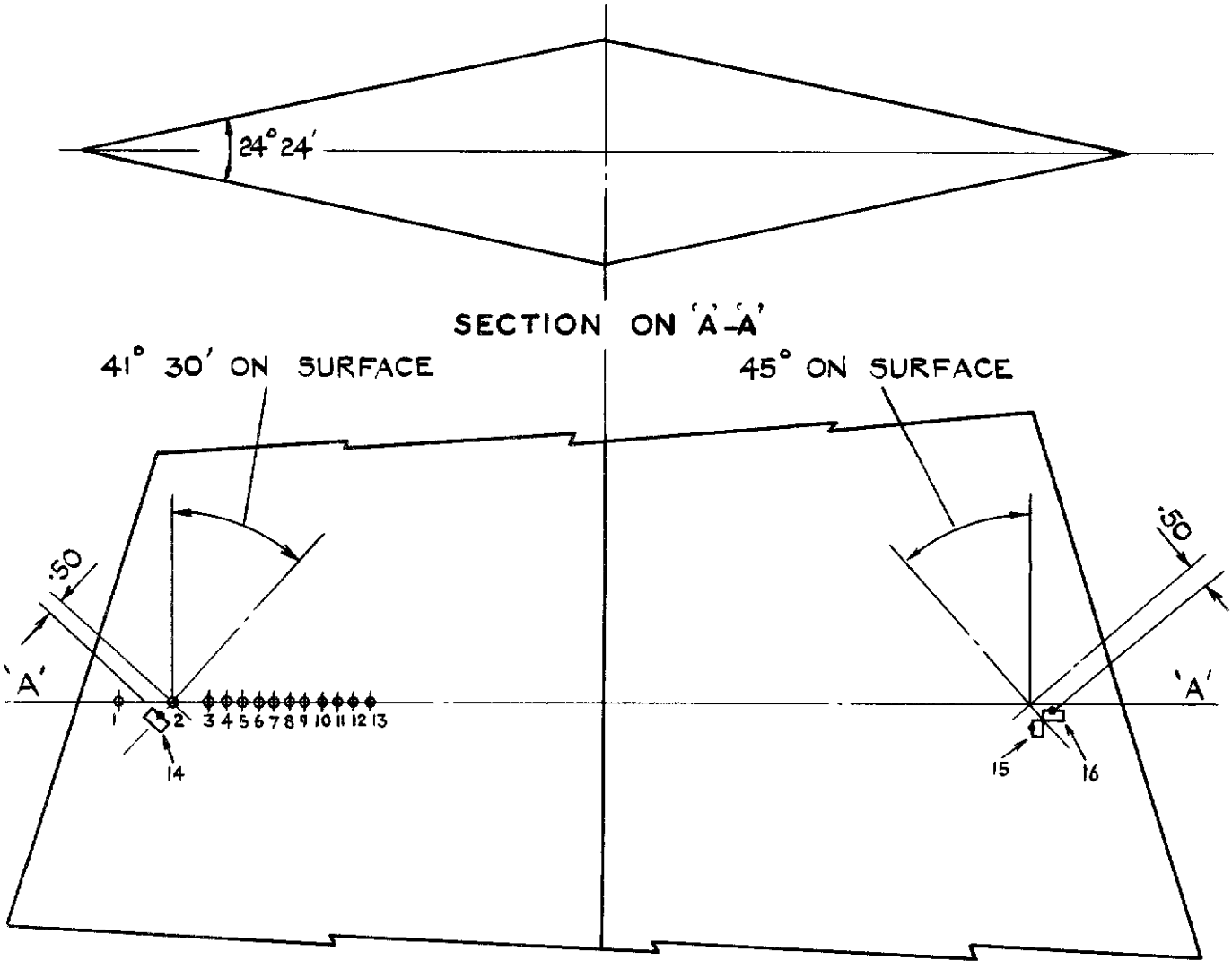

SCRAP PLAN VIEW OF CENTRE SECTION

STATIC PRESSURE MEASUREMENT POSITIONS													
POS^N	1	2	3	4	5	6	7	8	9	10	11	12	13
y/s	·90	·825	·750	·720	·70	·66	·63	60	57	·54	·51	·48	·45

SURFACE PITOT POSITIONS			
POS^N	14	15	16
y/s	·845	·834	·86

FIG. 3 PRESSURE-MEASUREMENT POSITIONS MODEL 4

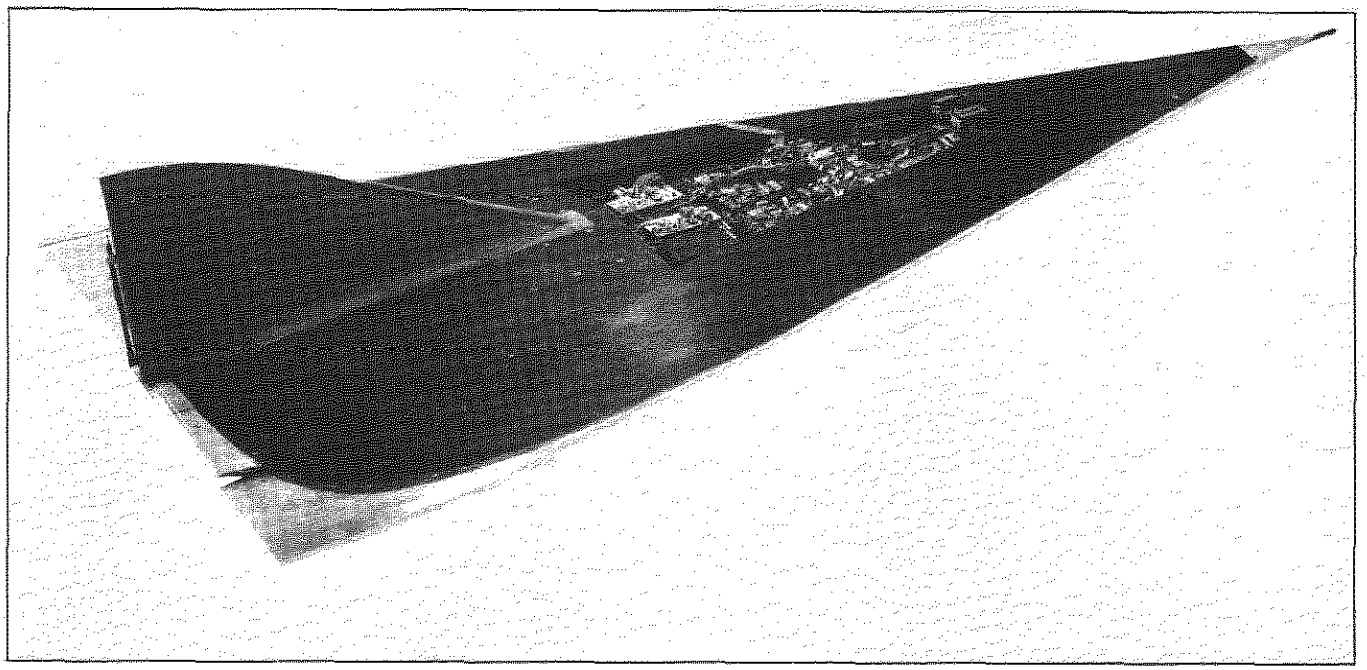

a. Complete model with instrumentation hatch removed

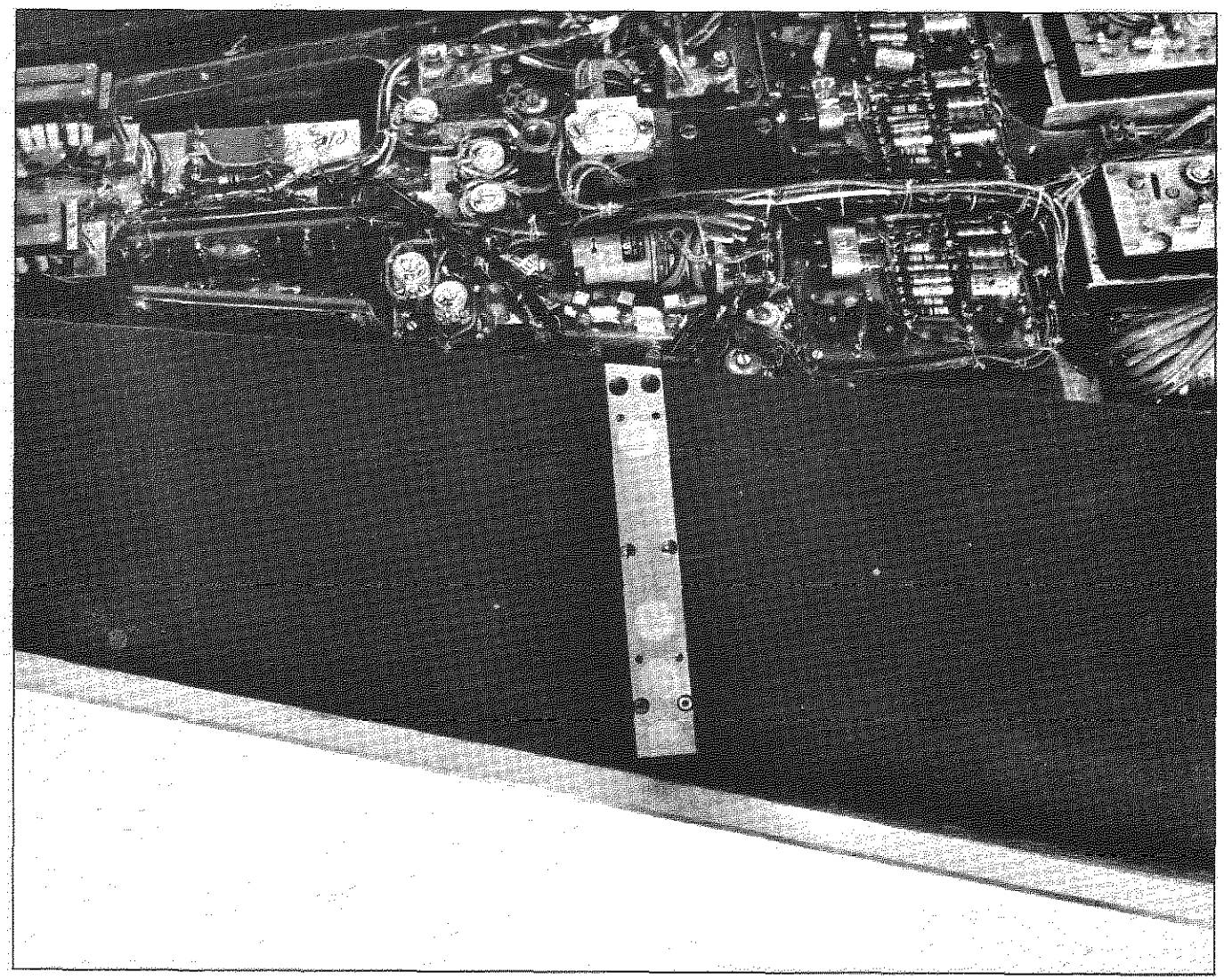

b. Mounting of pressure cells

Fig.4. Model 3

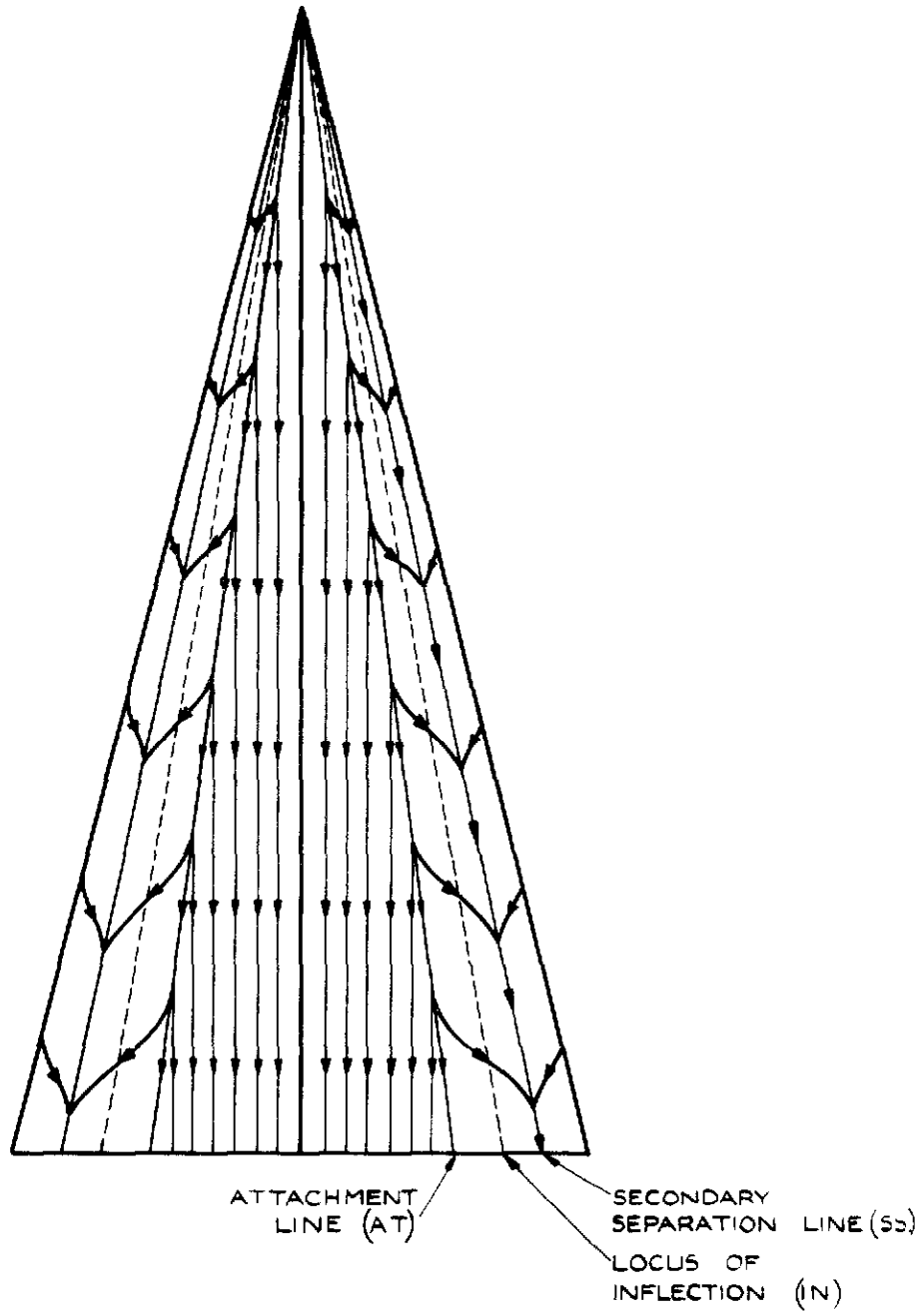

a SURFACE-FLOW PATTERN

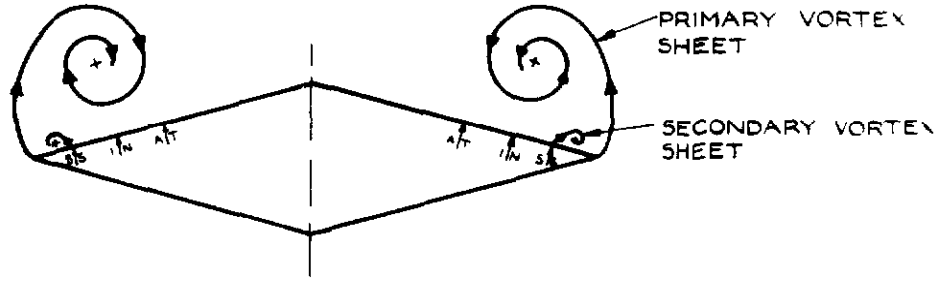

b CROSS-SECTION OF FLOW

FIG. 5 a & b FLOW OVER THE UPPER SURFACE OF A DELTA-WING AT INCIDENCE

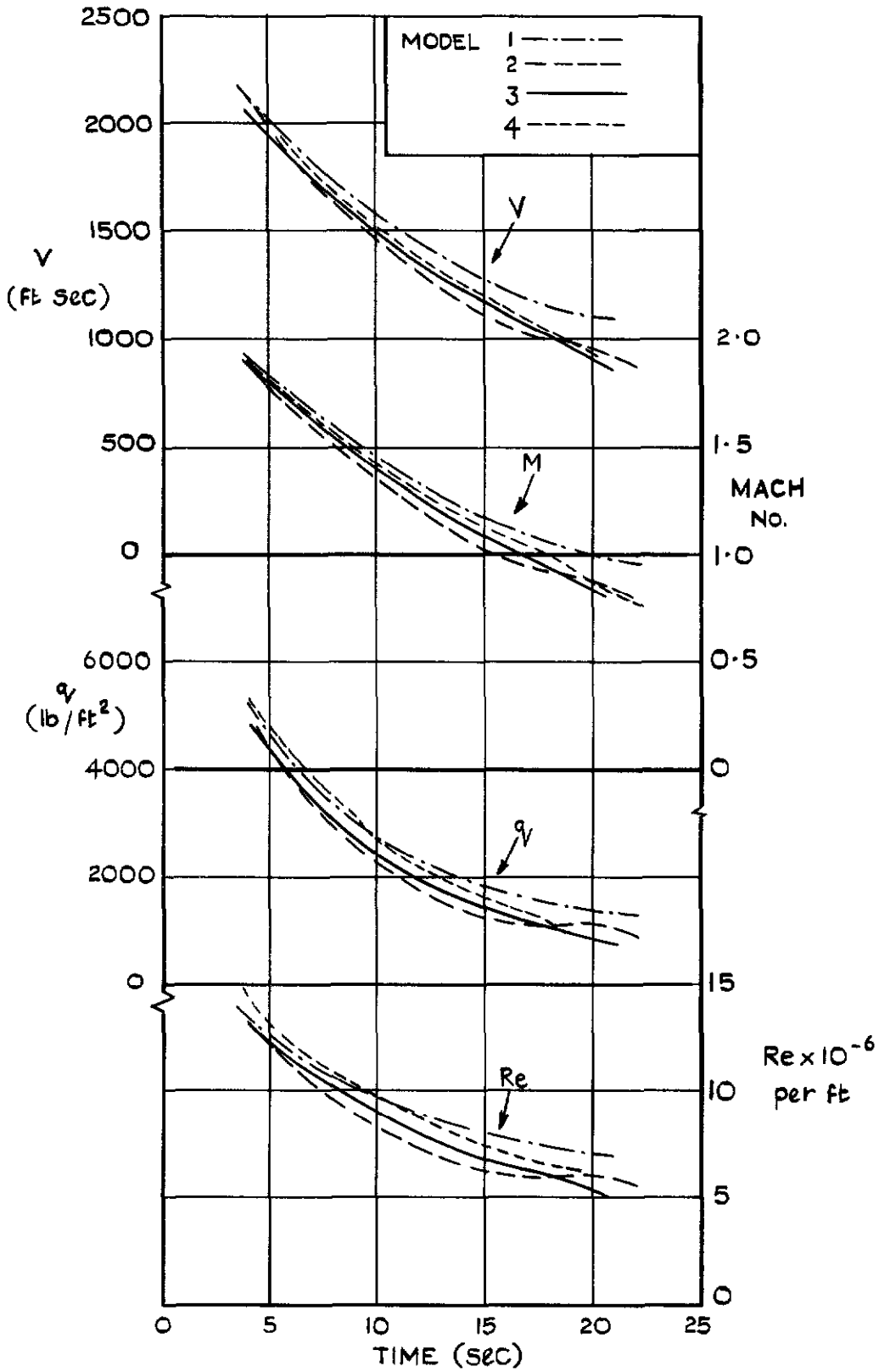

FIG. 6 FLIGHT PARAMETERS

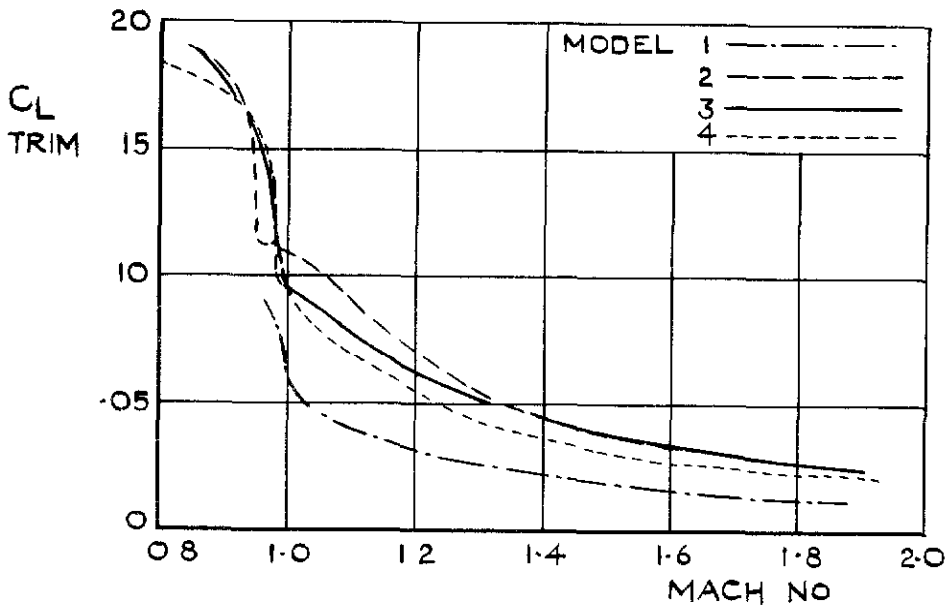

a TRIM LIFT COEFFICIENT

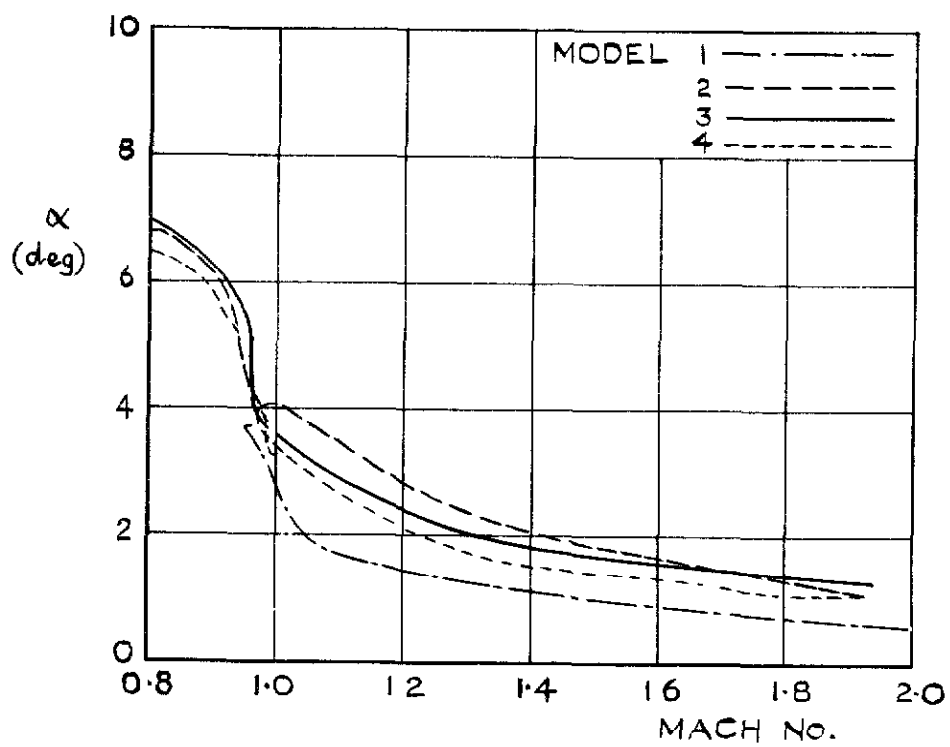

b TRIM INCIDENCE

FIG. 7 a & b TRIM CONDITIONS

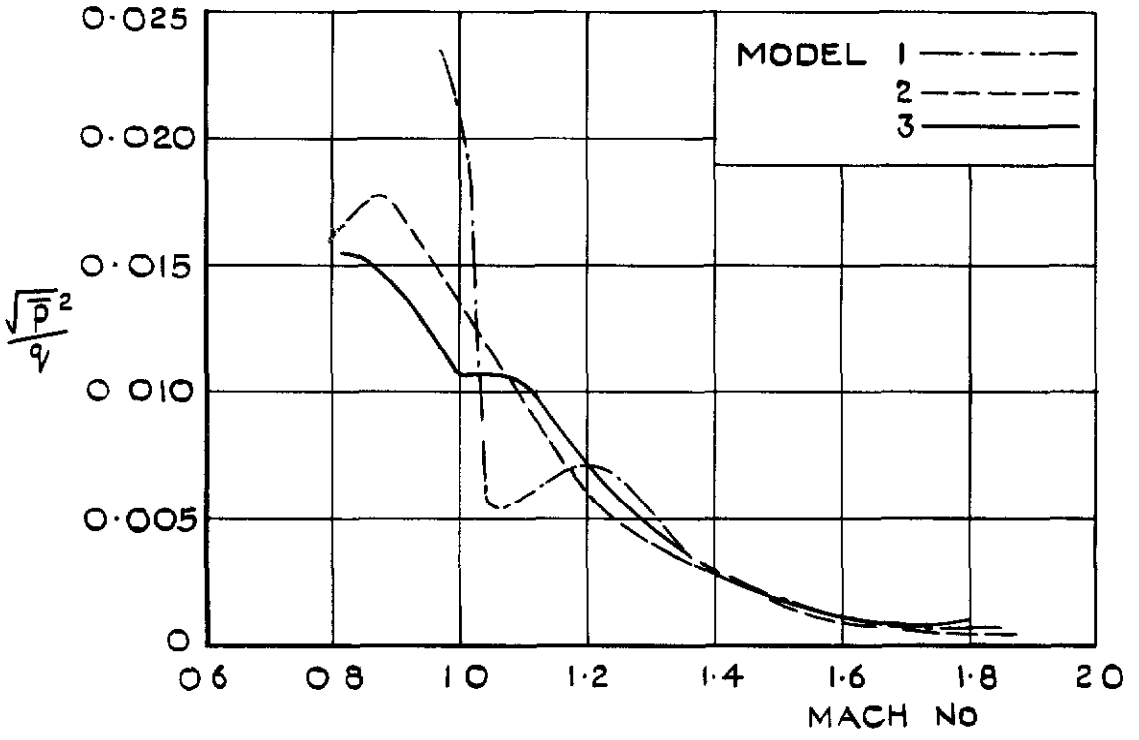

a COMPARISON FOR MODELS 1, 2, 3
$\frac{y}{s} \simeq 0 \cdot 083$

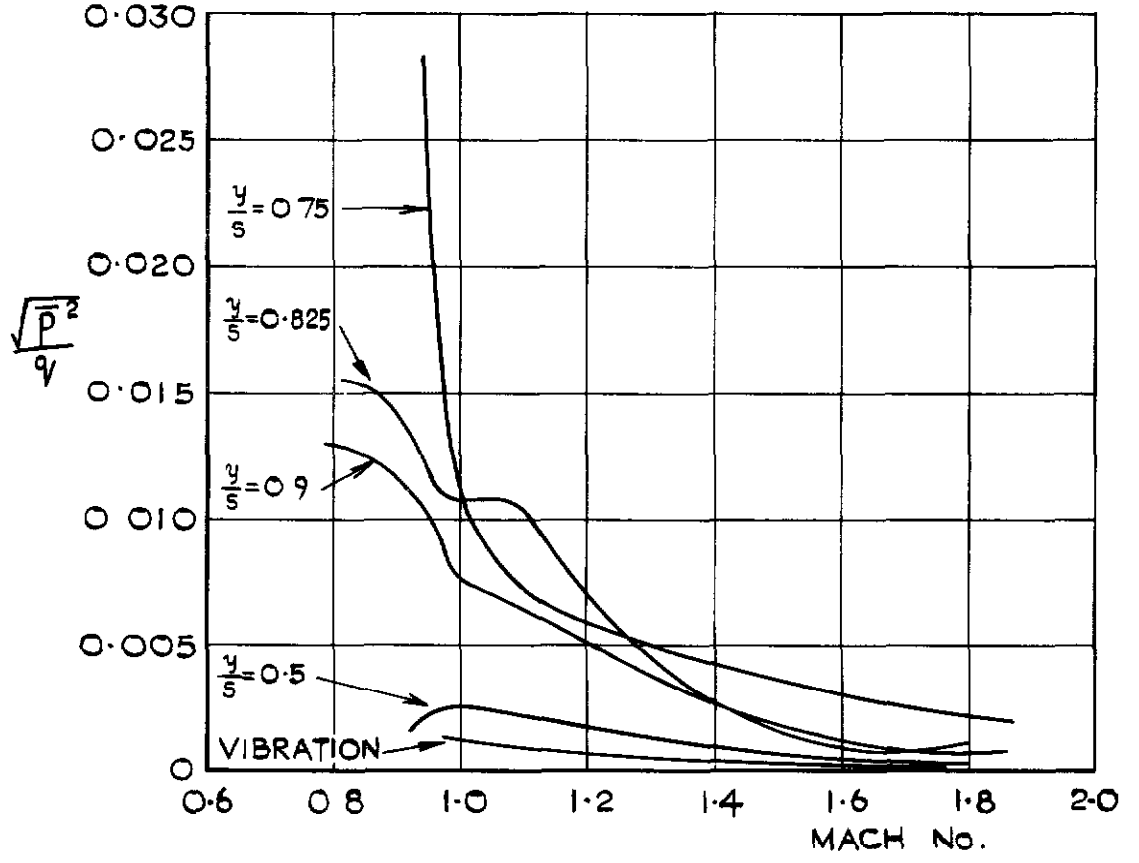

b SPANWISE DISTRIBUTION (MODEL 3)

FIG. 8 a&b R.M.S FLUCTUATING PRESSURE COEFFICIENTS
(BANDWIDTH 200 c/s TO 20 kc/s)

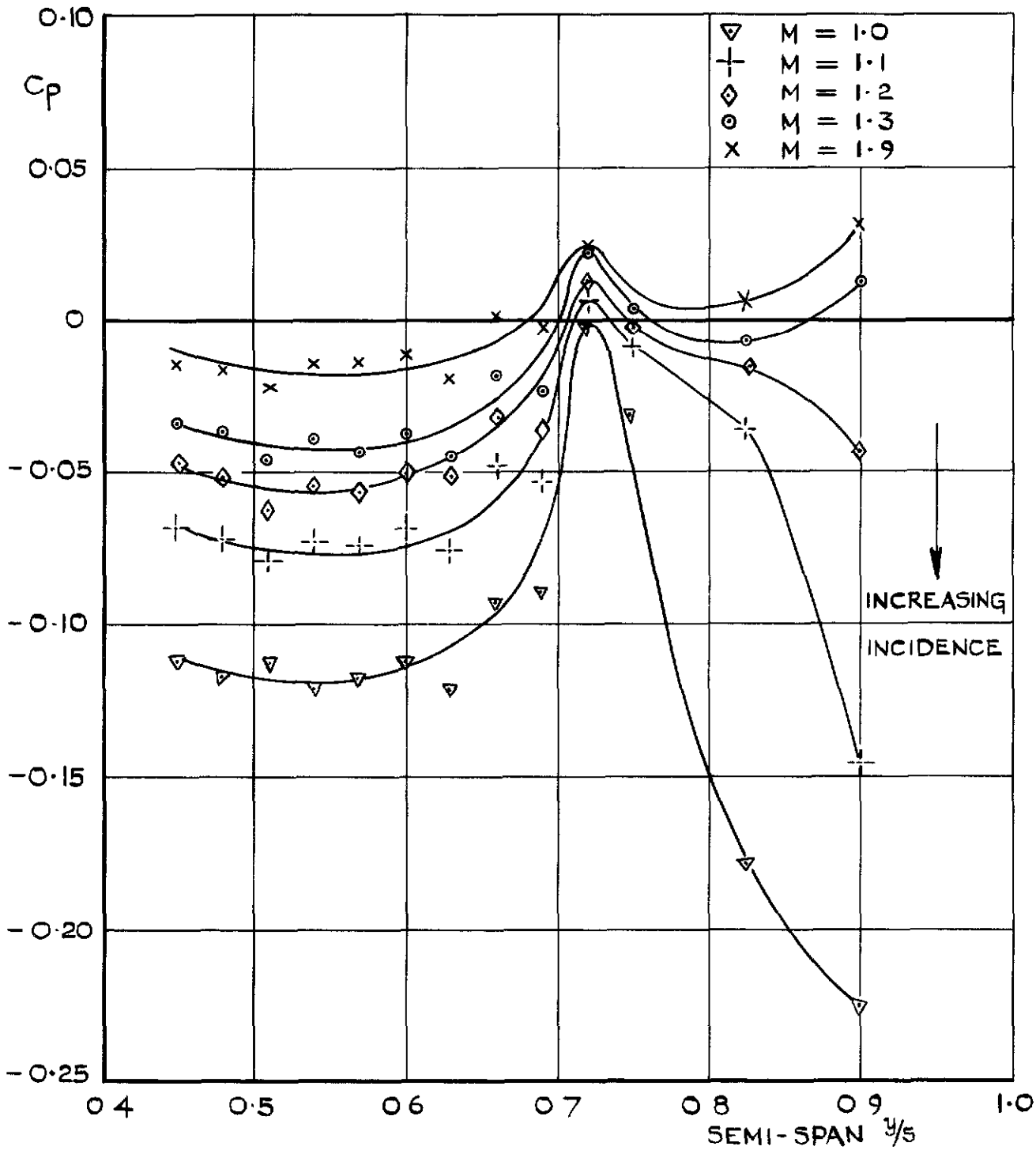

FIG.9 SPANWISE STATIC PRESSURE DISTRIBUTION (MODEL 4)

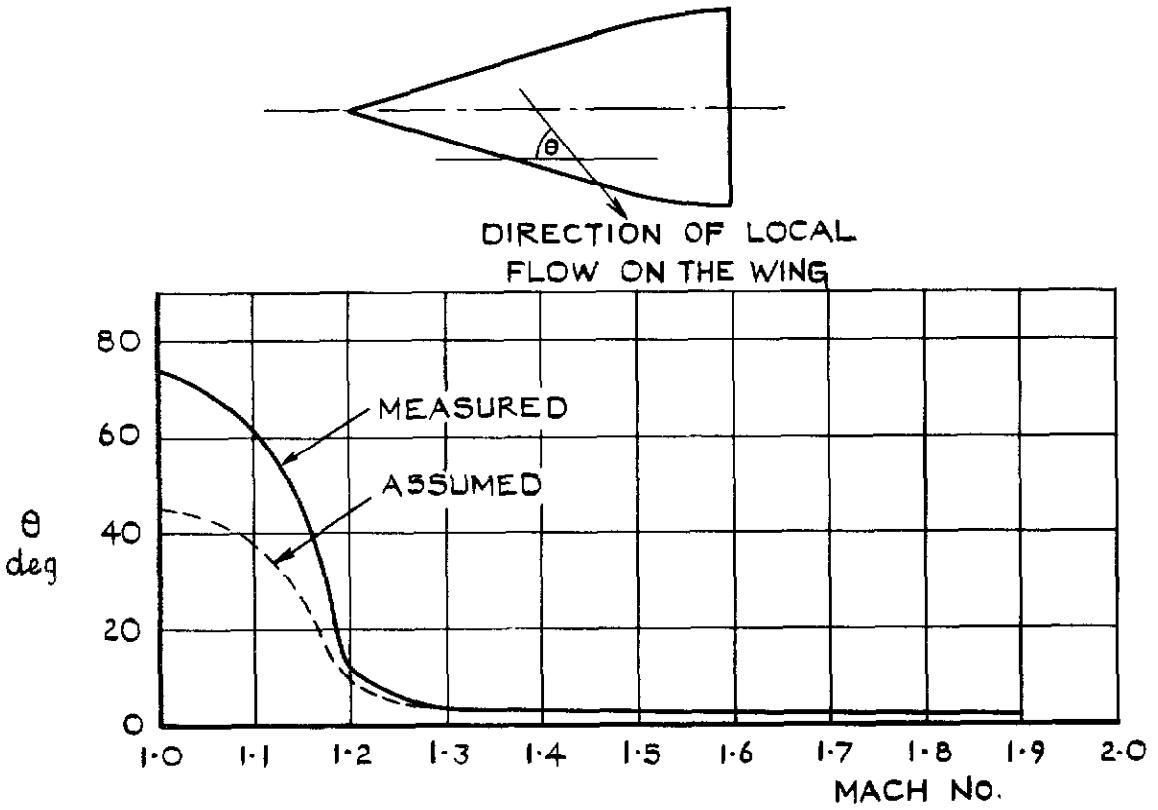

a VARIATION WITH MACH No.

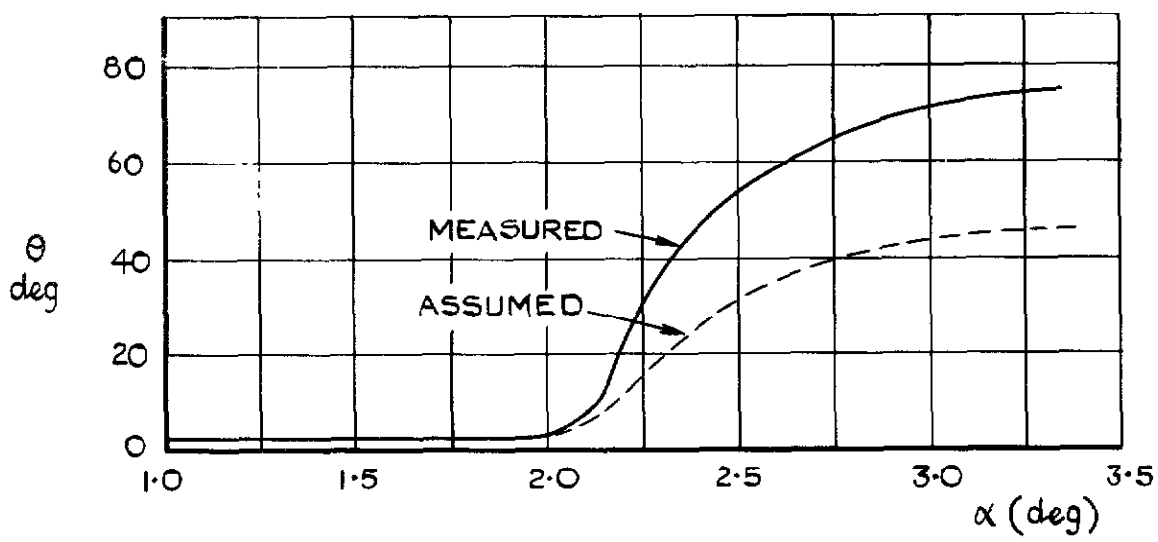

b VARIATION WITH INCIDENCE

FIG.10a&b LOCAL FLOW DIRECTION AT $y/s = 0.825$ (MODEL 4)

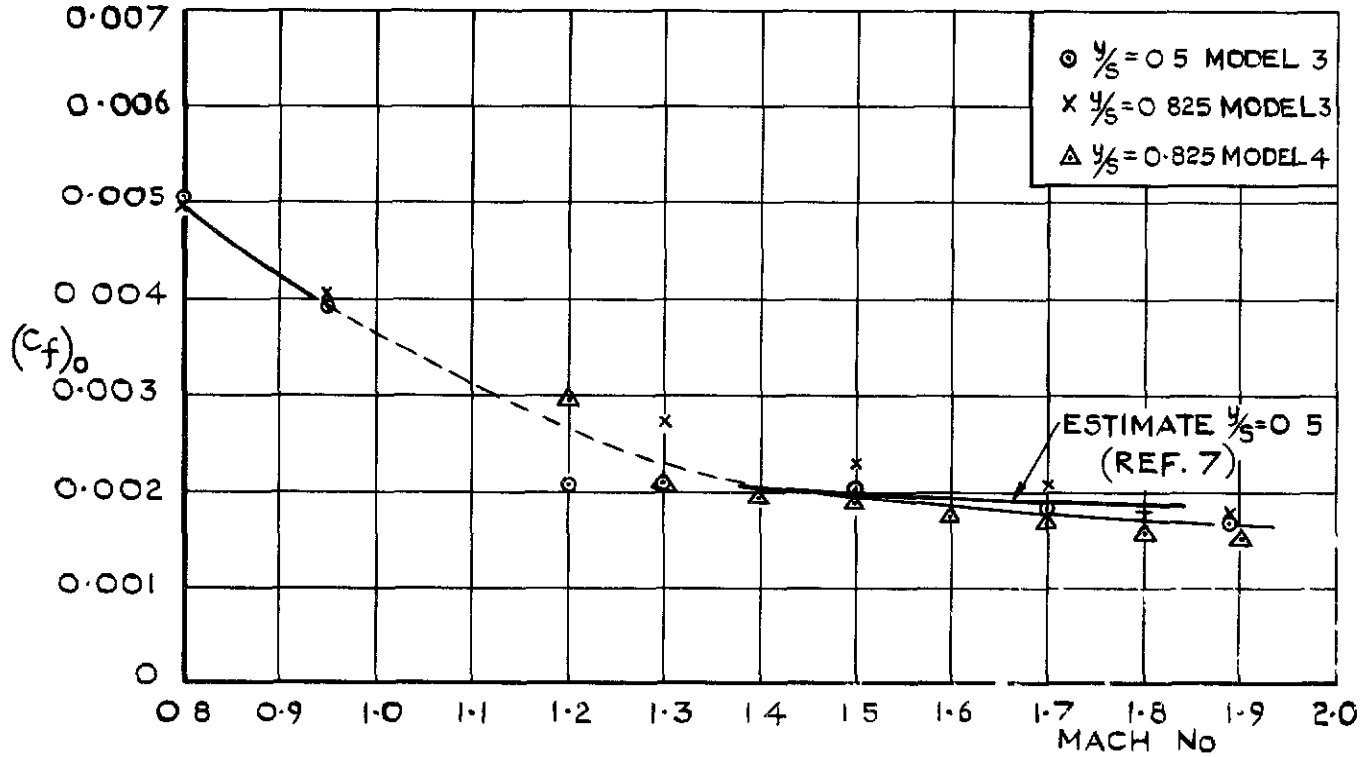

a COMPONENT IN FREE STREAM DIRECTION

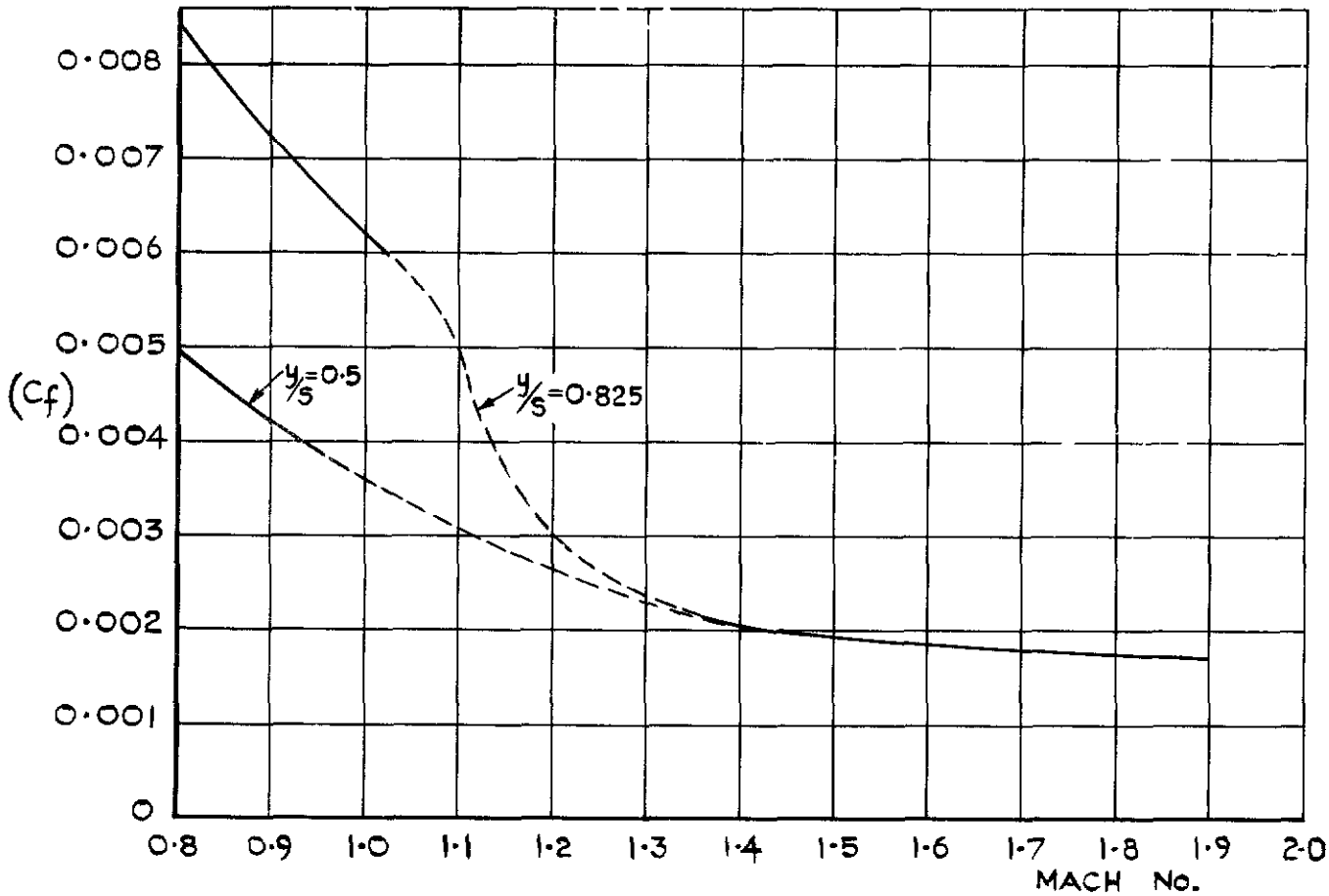

b COMPONENT IN LOCAL FLOW DIRECTION

FIG. 11 a & b LOCAL SKIN FRICTION COEFFICIENTS

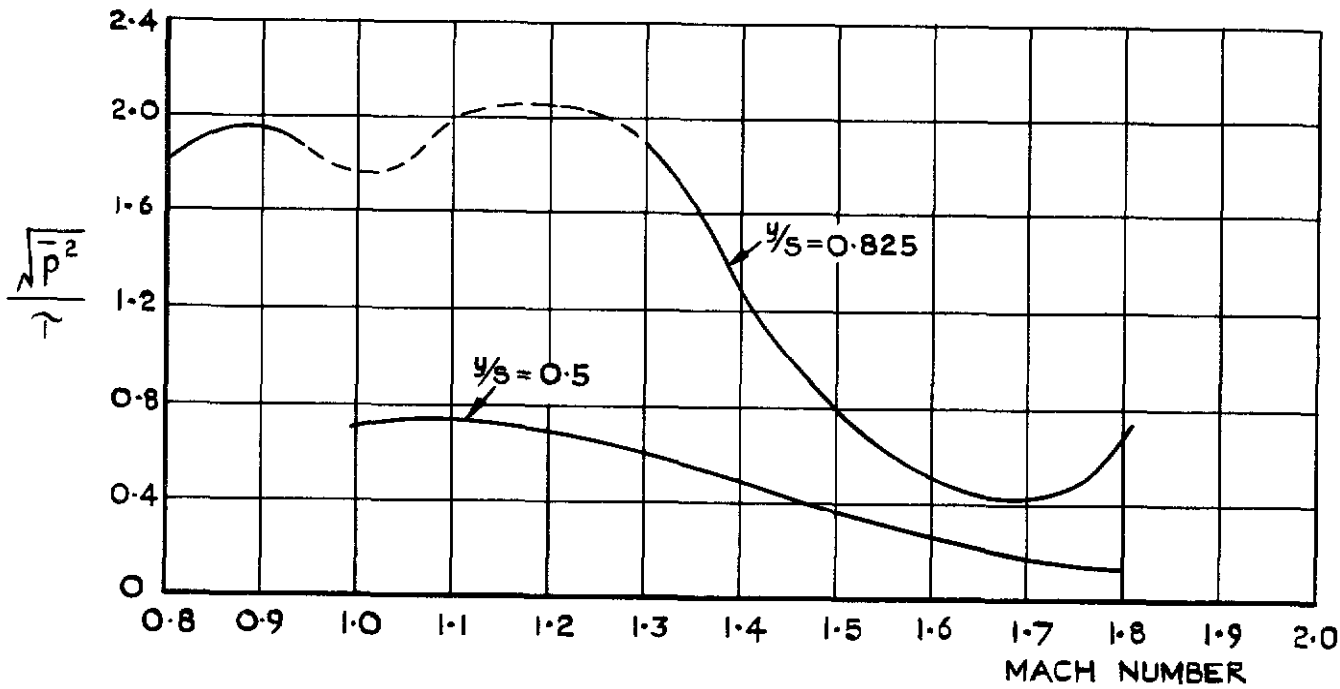

FIG. 12 RATIO OF R.M.S PRESSURE TO LOCAL SKIN FRICTION $y/s = 0·825$ (MODEL 3); R.M.S PRESSURE IN BAND 200 c/s TO 20 kc/s

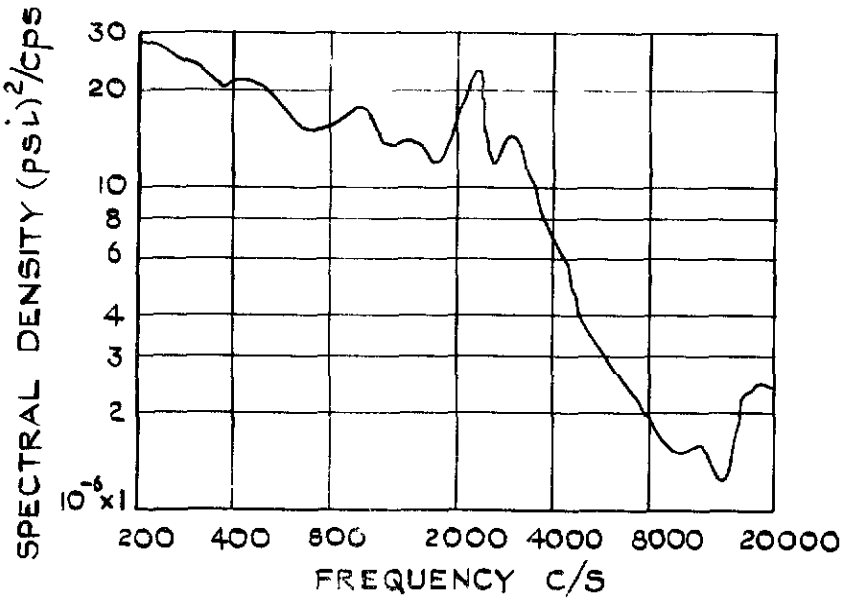

MODEL 1
M = 0·97
y/s = 0·84

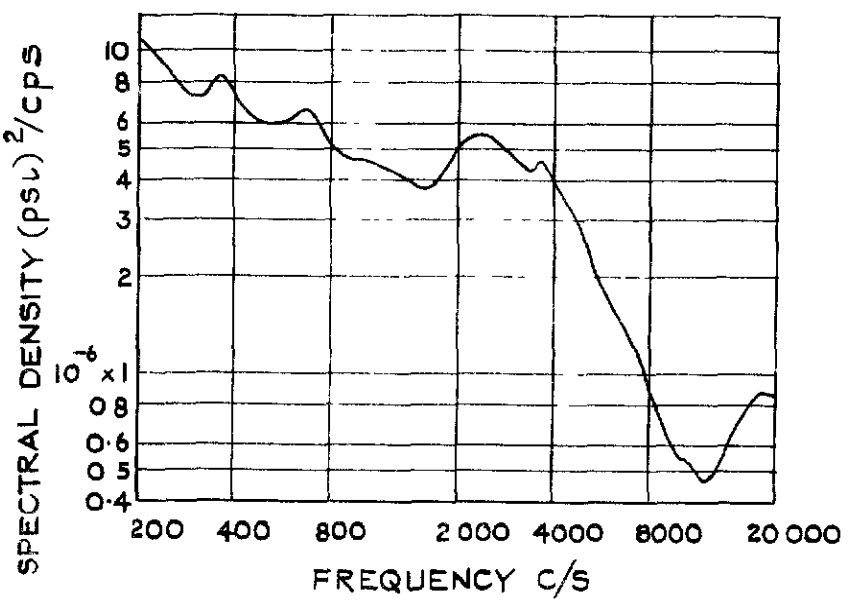

MODEL 2
M = 0·93
y/s = 0·84

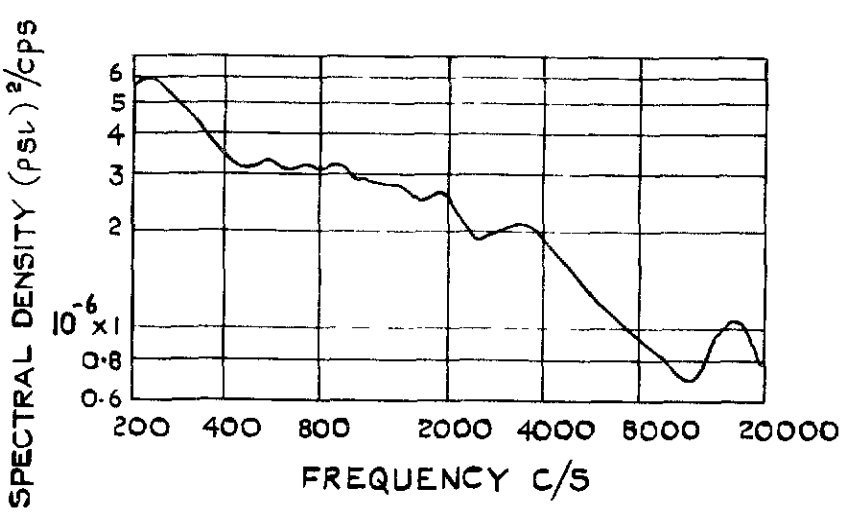

MODEL 3
M = 0 93
y/s = 0·825

a MACH NUMBER APPROX. 0·95

FIG.13a SPECTRAL DENSITY COMPARISON FOR MODELS 1, 2, 3

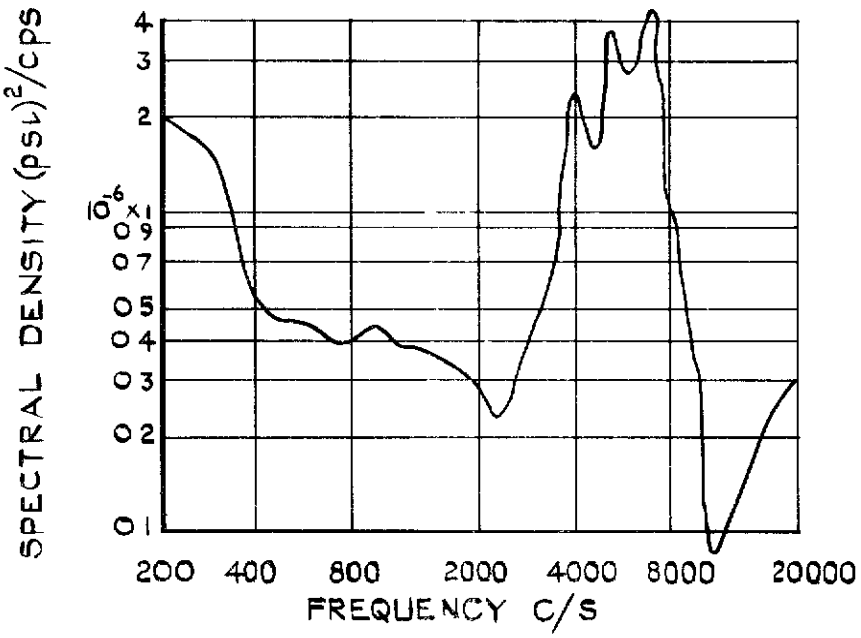

MODEL 1

M = 1·19

y/s = 0·84

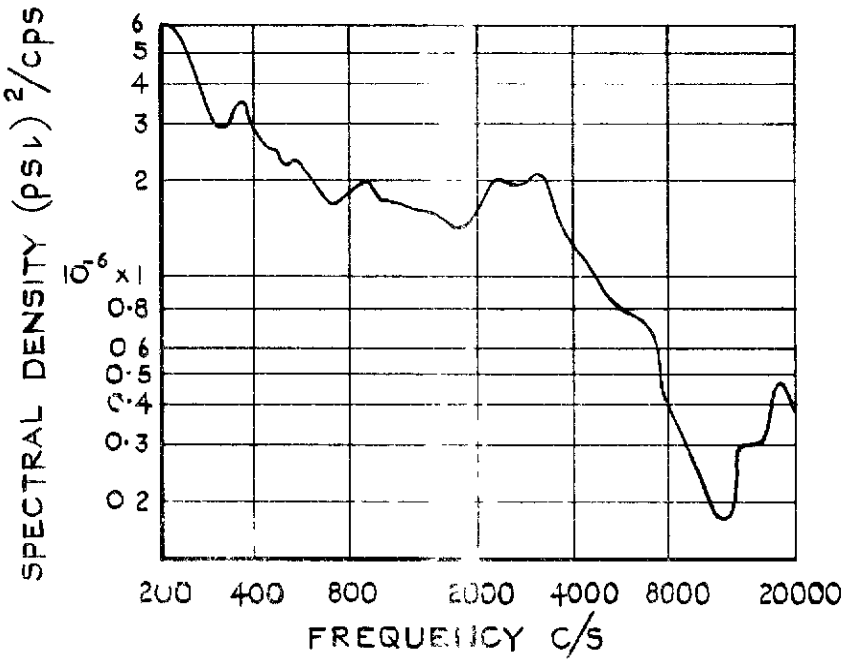

MODEL 2

M = 1·21

y/s = 0·84

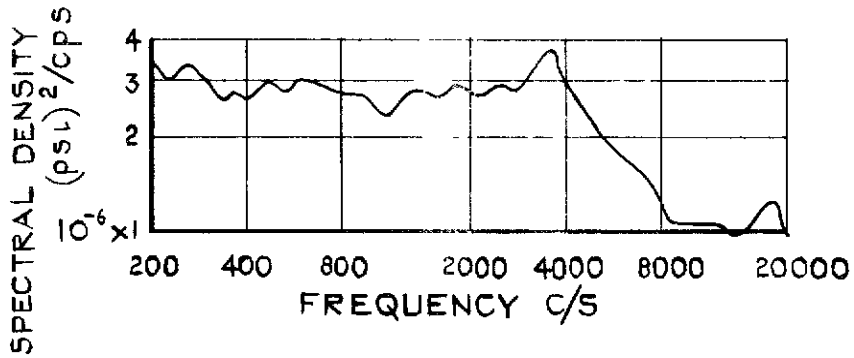

MODEL 3

M = 1·09

y/s = 0 825

b MACH NUMBER APPROX 1·20

FIG. 13 b SPECTRAL DENSITY COMPARISON FOR MODEL 1, 2, 3

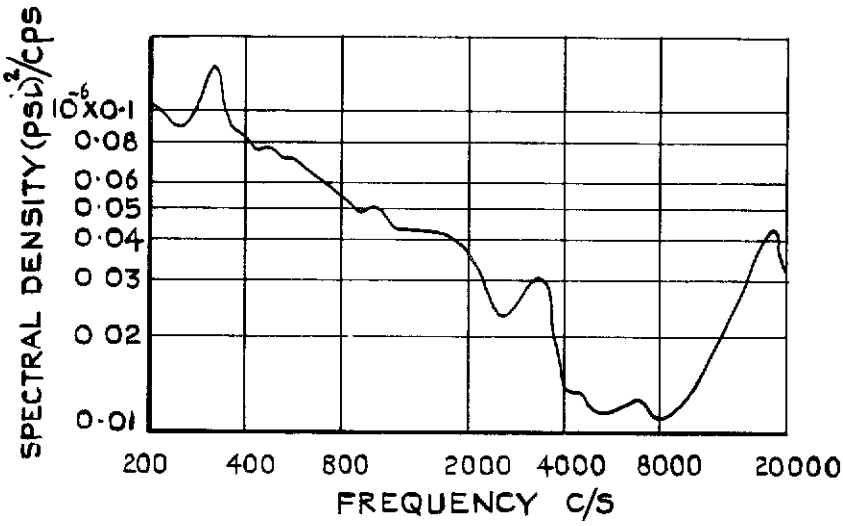

$y/s = 0\,5$

$M = 0{\cdot}93$

RMS PRESSURE
$= 0{\cdot}012$ psi

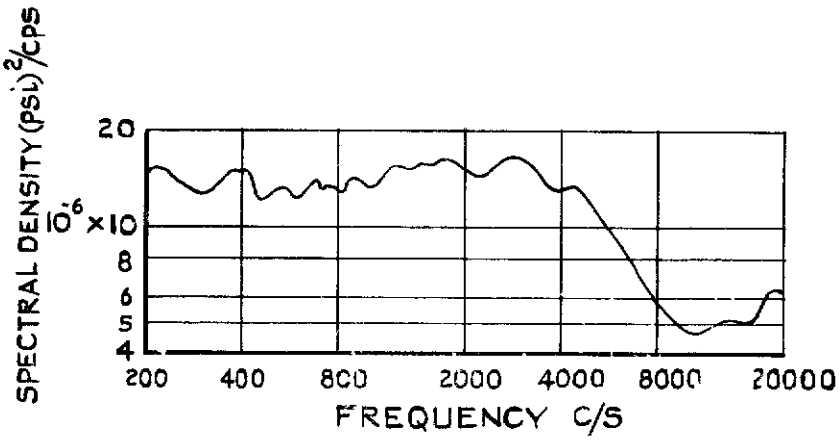

$y/s = 0{\cdot}75$

$M = 0{\cdot}96$

RMS PRESSURE
$= 0{\cdot}217$ psi

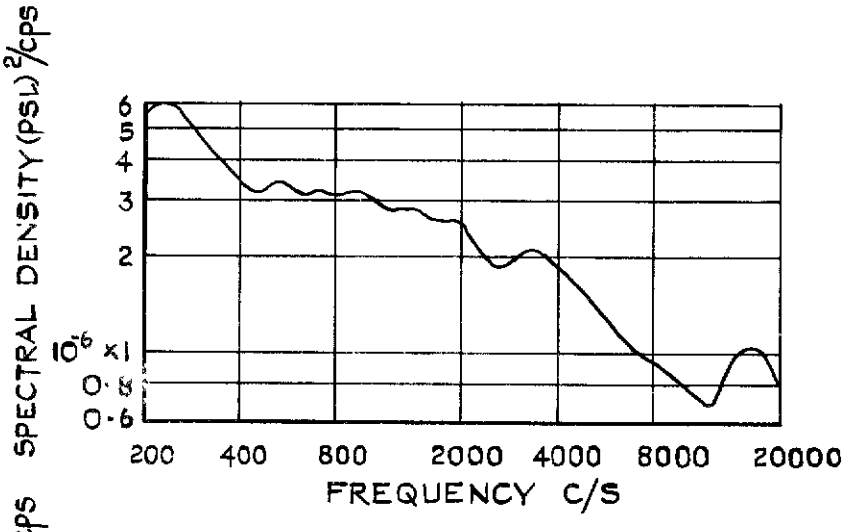

$y/s = 0\ 825$

$M = 0{\cdot}93$

RMS PRESSURE
$= 0\ 095$ psi

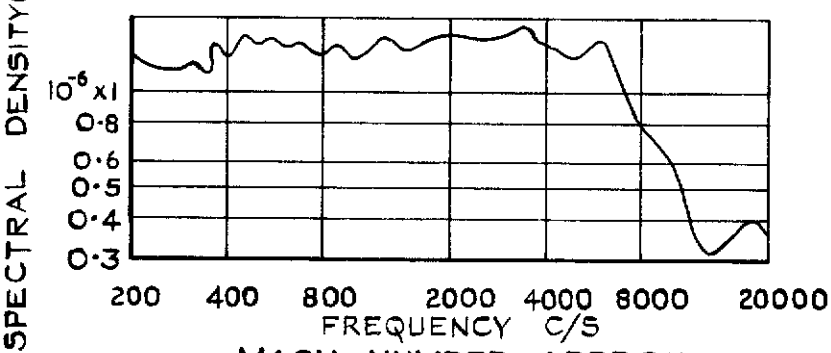

$y/s = 0{\cdot}9$

$M = 0{\cdot}96$

RMS PRESSURE
$= 0{\cdot}076$ psi

a MACH NUMBER APPROX 0·95

FIG.14 a SPANWISE DISTRIBUTION OF SPECTRAL DENSITY (MODEL 3)

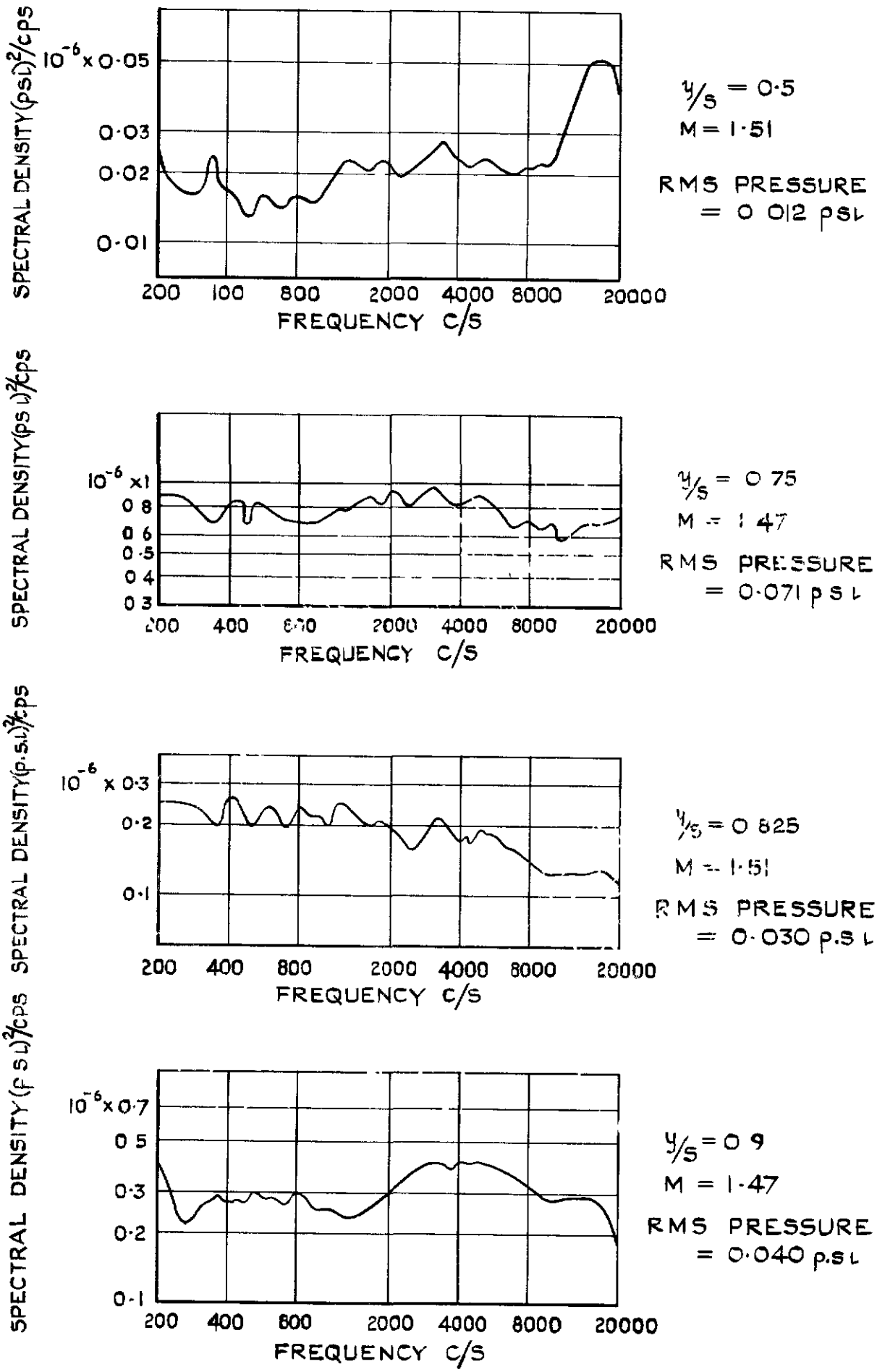

b MACH NUMBER APPROX 1·5

FIG 14 b SPANWISE DISTRIBUTION OF SPECTRAL DENSITY (MODEL 3)

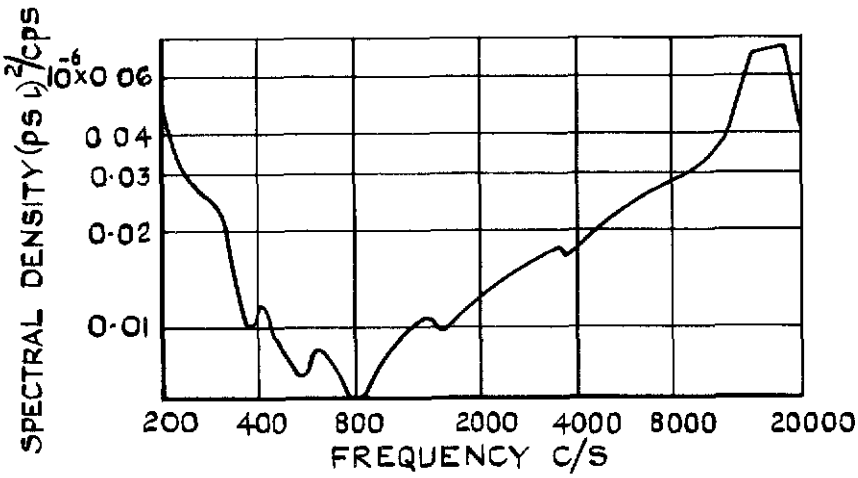

$y/s = 0.5$

$M = 1.80$

RMS PRESSURE
= 0 007 psi

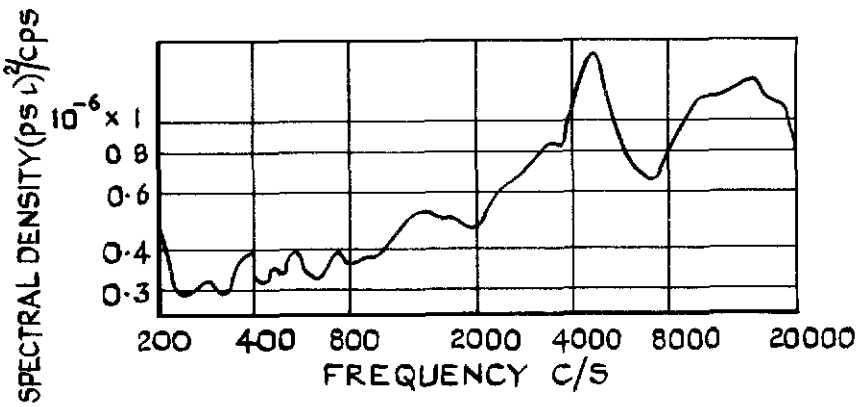

$y/s = 0.75$

$M = 1.86$

RMS PRESSURES
= 0 068 psi

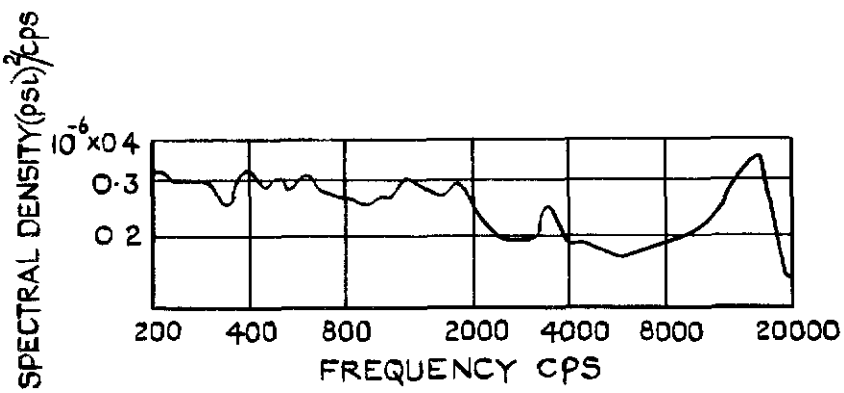

$y/s = 0.825$

$M = 1.80$

RMS PRESSURE
= 0·036 psi

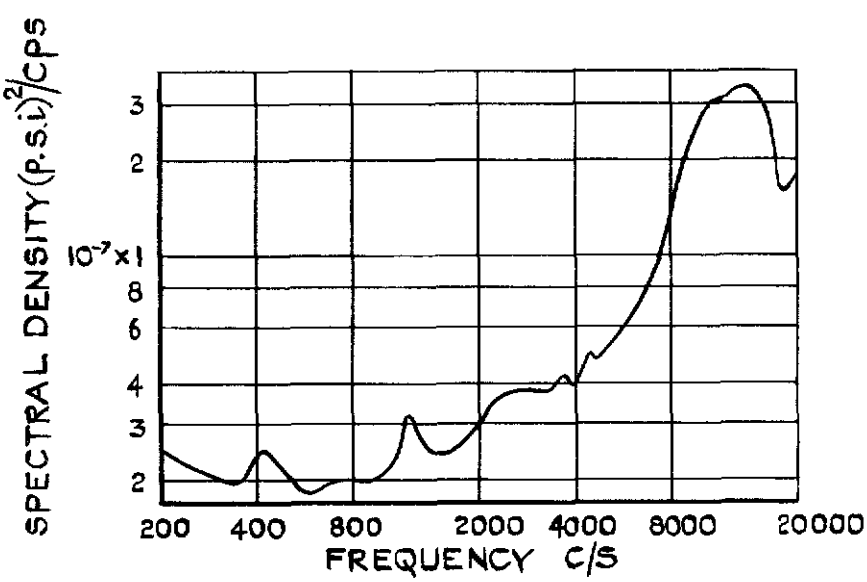

$y/s = 0.9$

$M = 1.86$

RMS PRESSURE
= 0·028 psi

c MACH NUMBER APPROX 1·85

FIG.14 c SPANWISE DISTRIBUTION OF SPECTRAL DENSITY (MODEL 3)

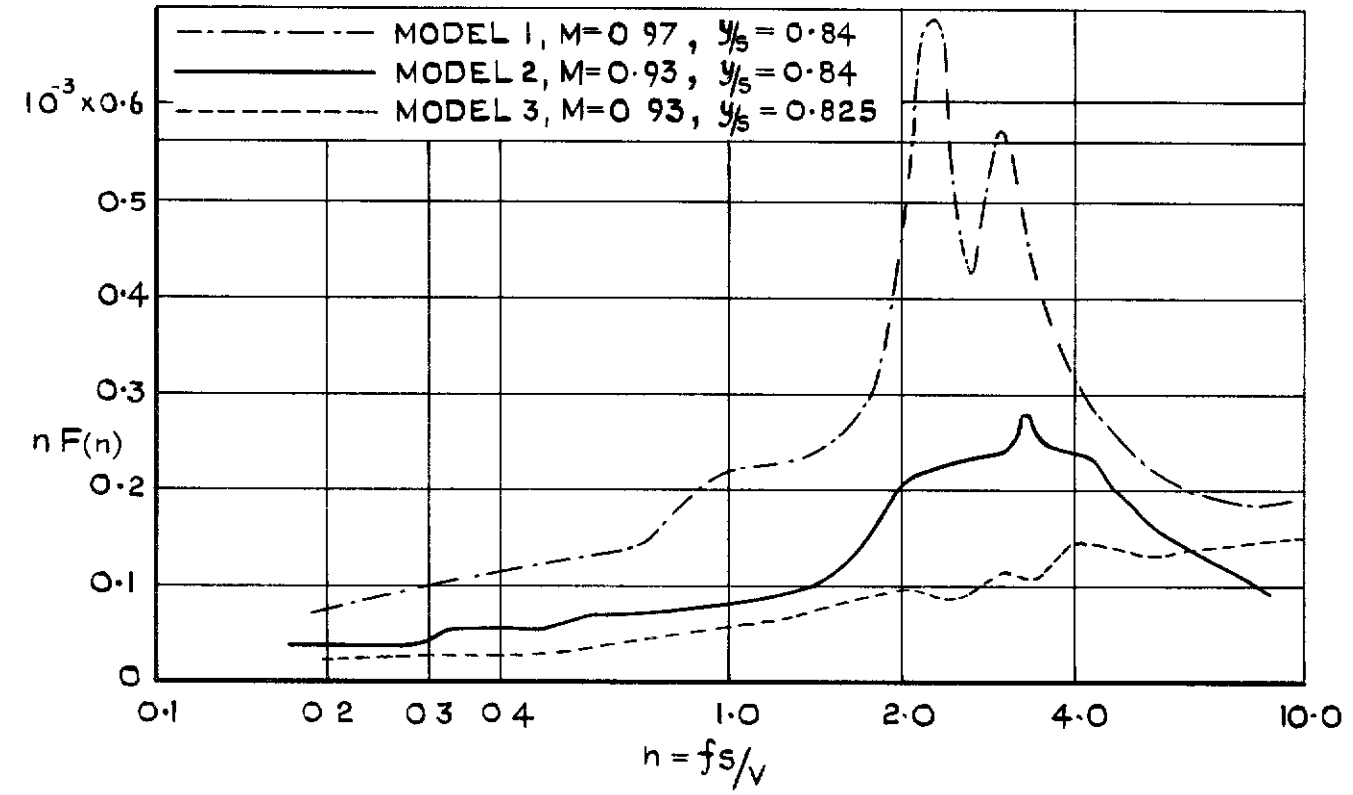

a MACH NUMBER APPROX. 0·95

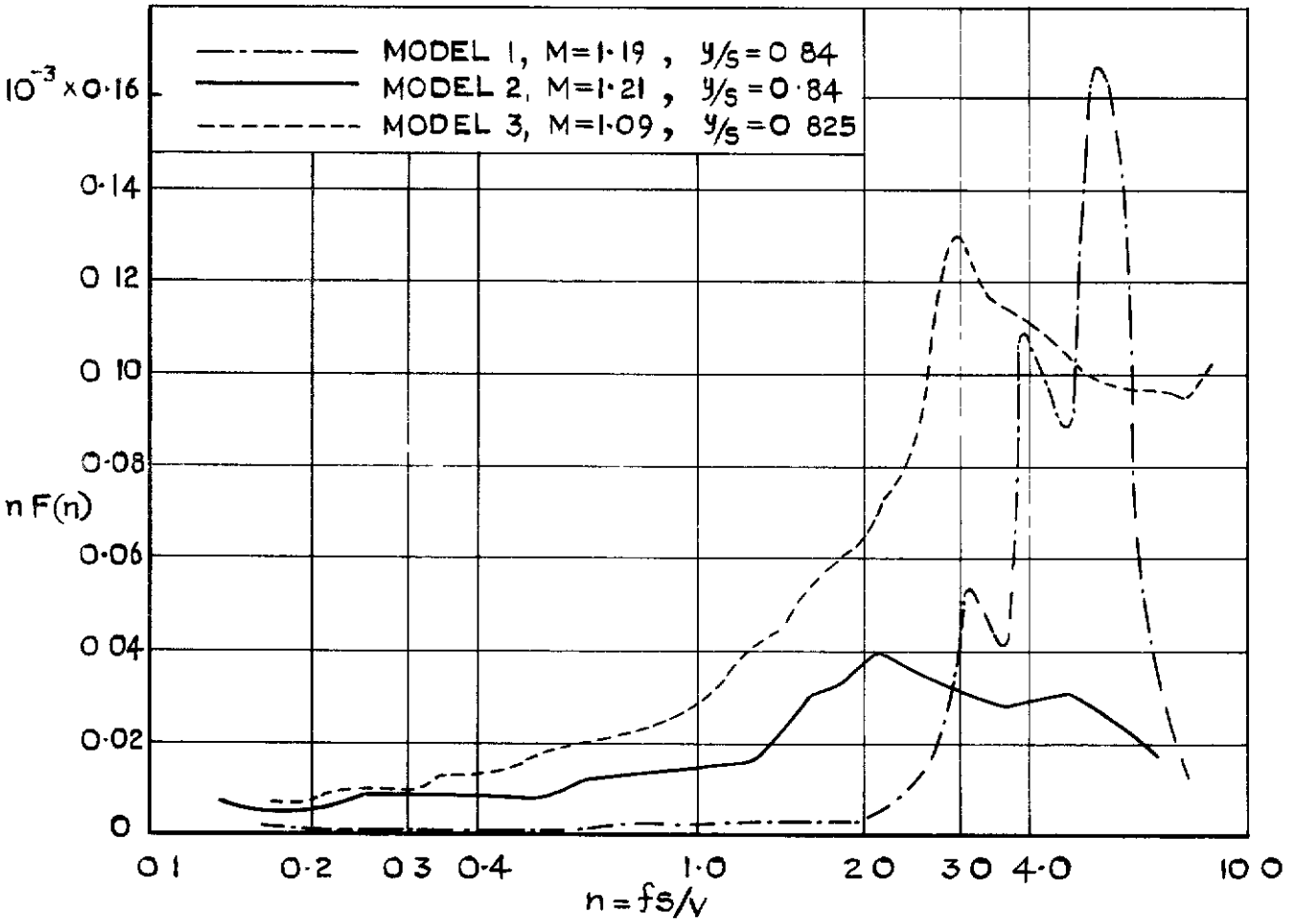

b MACH NUMBER APPROX 1·2

FIG.15 a & b NON DIMENSIONALISED SPECTRAL DENSITY COMPARISON FOR MODELS 1,2,3

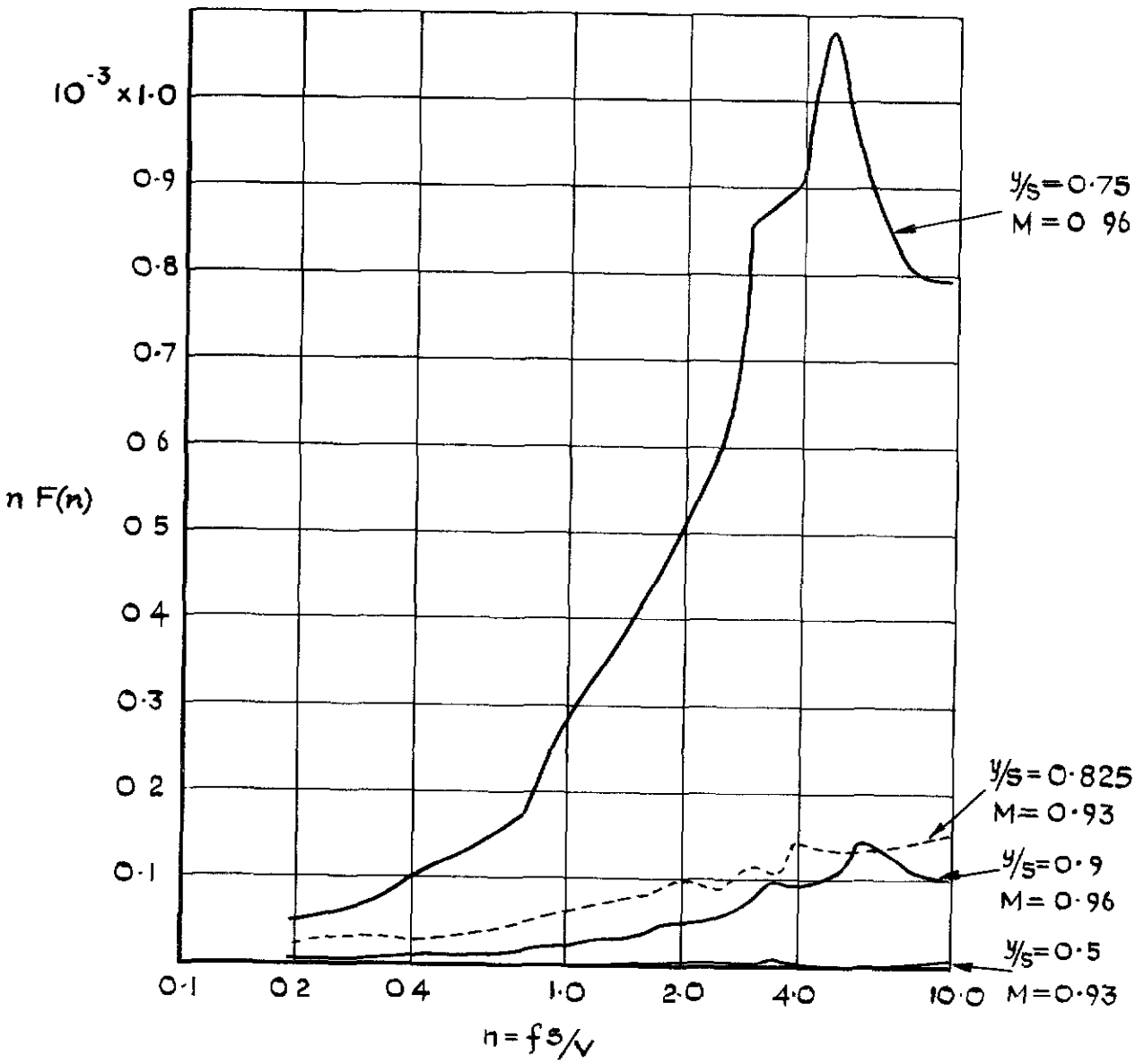

a MACH NUMBER APPROX 0·95

FIG.16 a SPANWISE DISTRIBUTION OF NON-DIMENSIONALISED SPECTRAL DENSITY (MODEL 3)

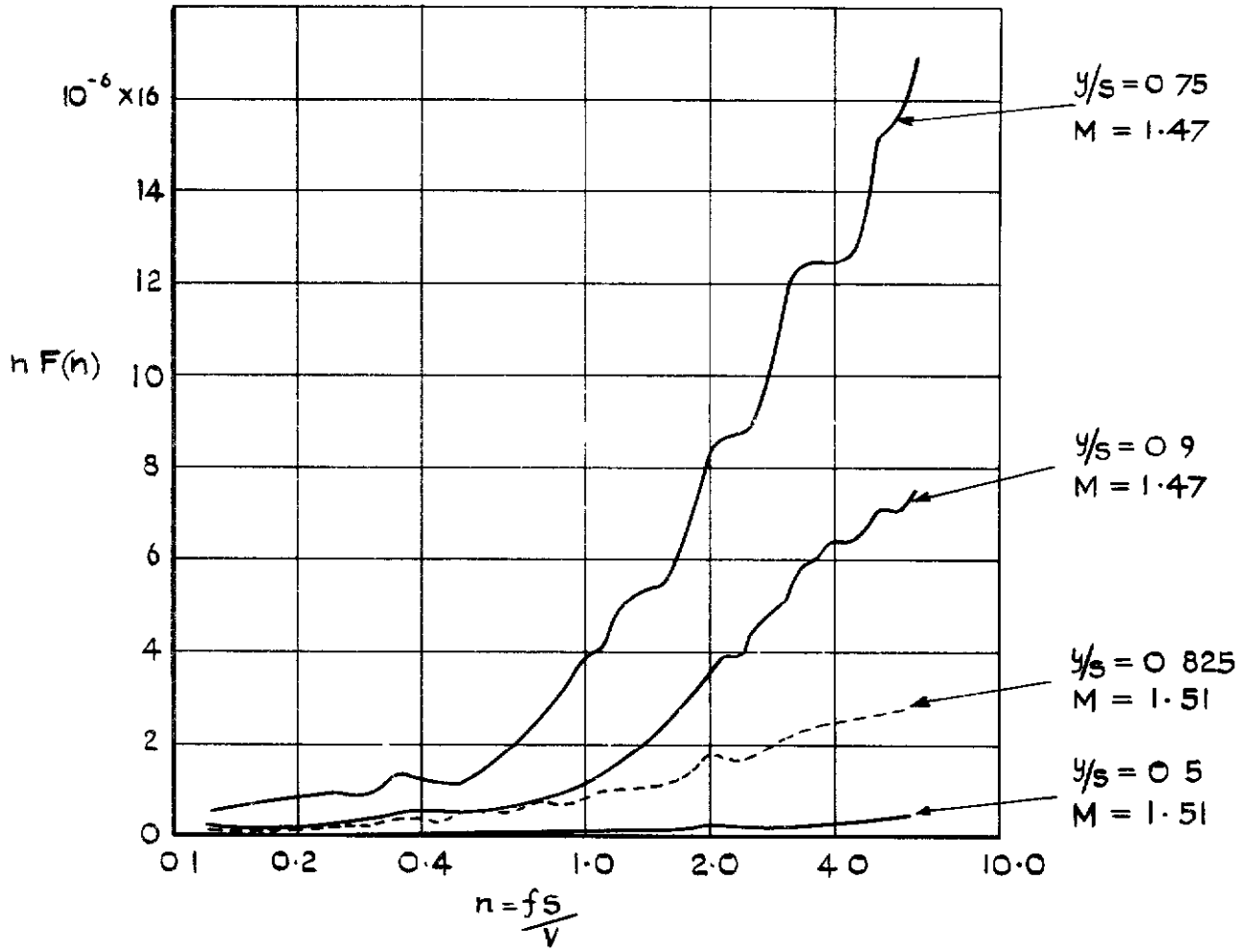

b MACH NUMBER APPROX 1·5

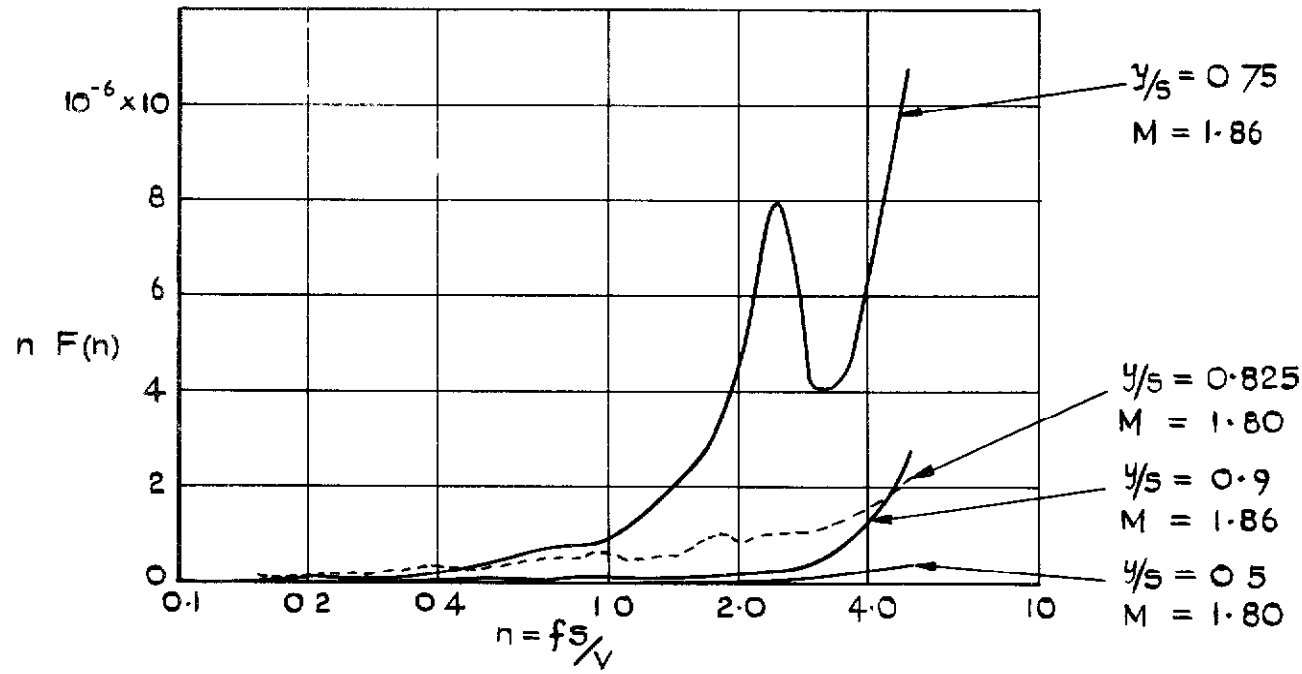

c MACH NUMBER APPROX 1·85

FIG.16 b&c SPANWISE DISTRIBUTION OF NON-DIMENSIONALISED SPECTRAL DENSITY (MODEL 3)

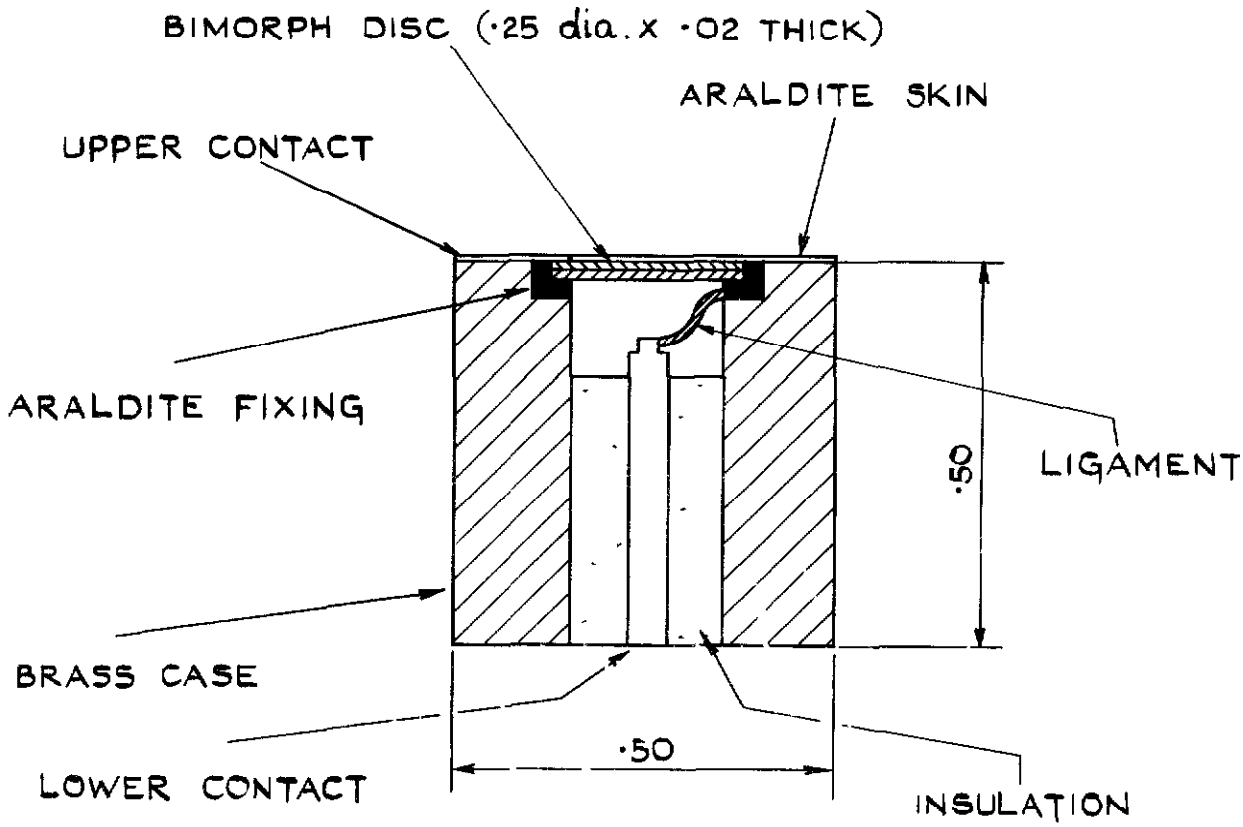

a RIM CLAMPED TRANSDUCER MODEL 1

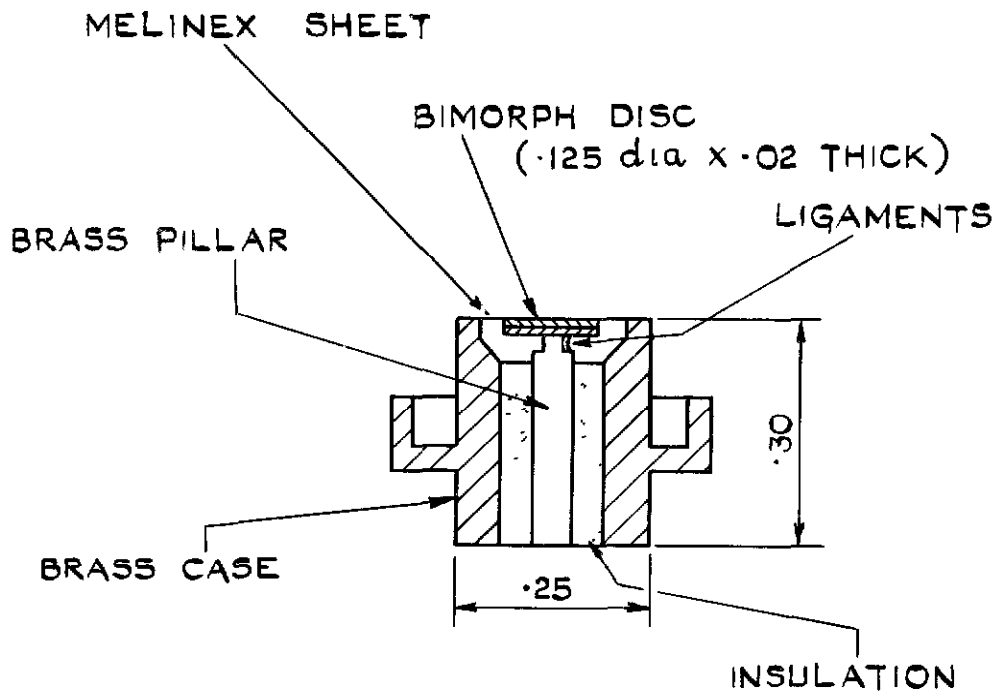

b CENTRE SUPPORTED TRANSDUCER MODELS 2 & 3

FIG. 17 a & b TRANSDUCERS

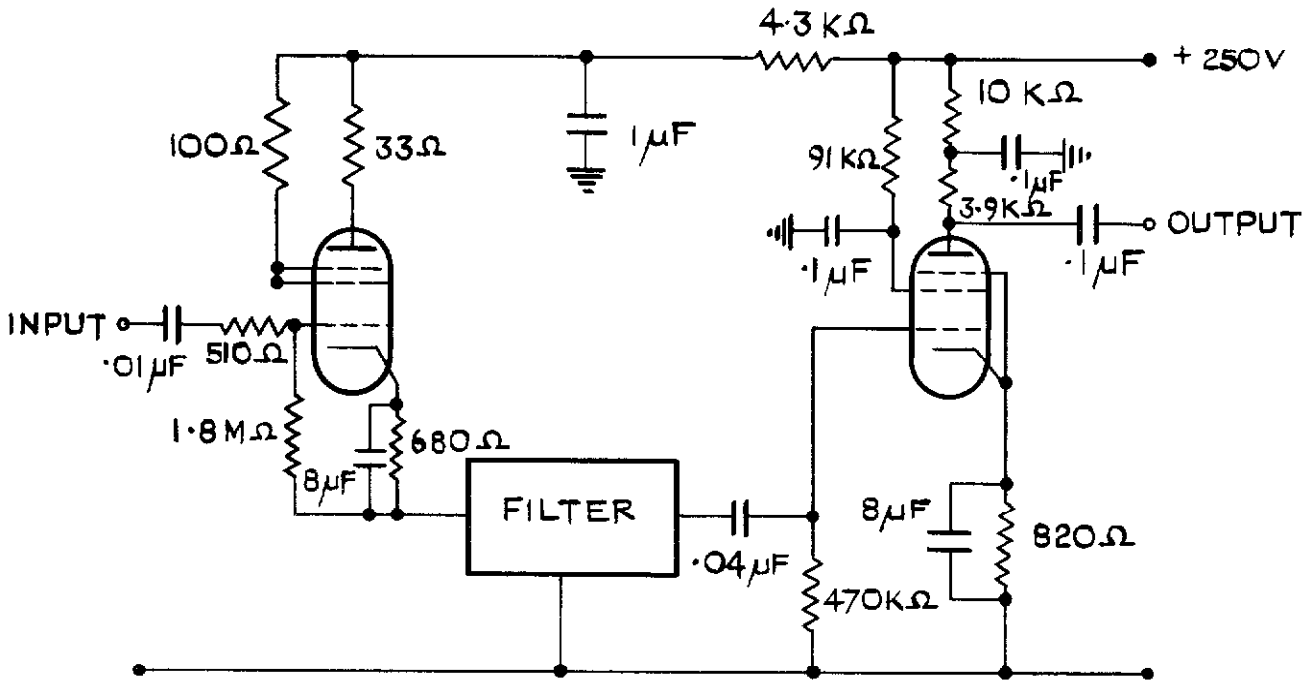

a CATHODE FOLLOWER AND AMPLIFIER

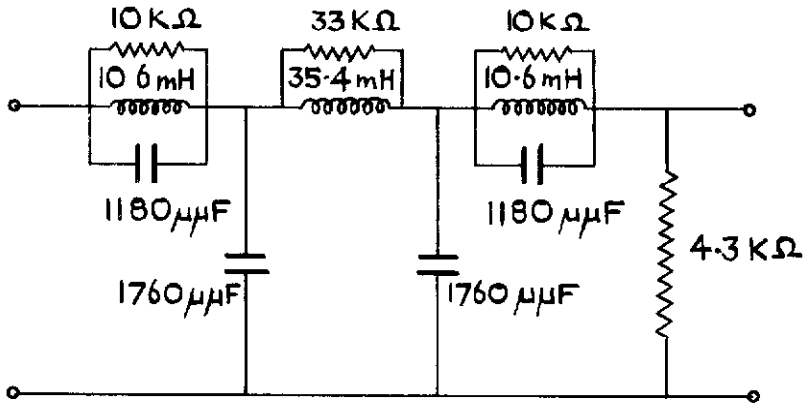

b 45 Kc/s CUT-OFF FILTER

FIG.18 a & b CATHODE FOLLOWER FILTER AND AMPLIFIER CIRCUIT FOR MODEL I

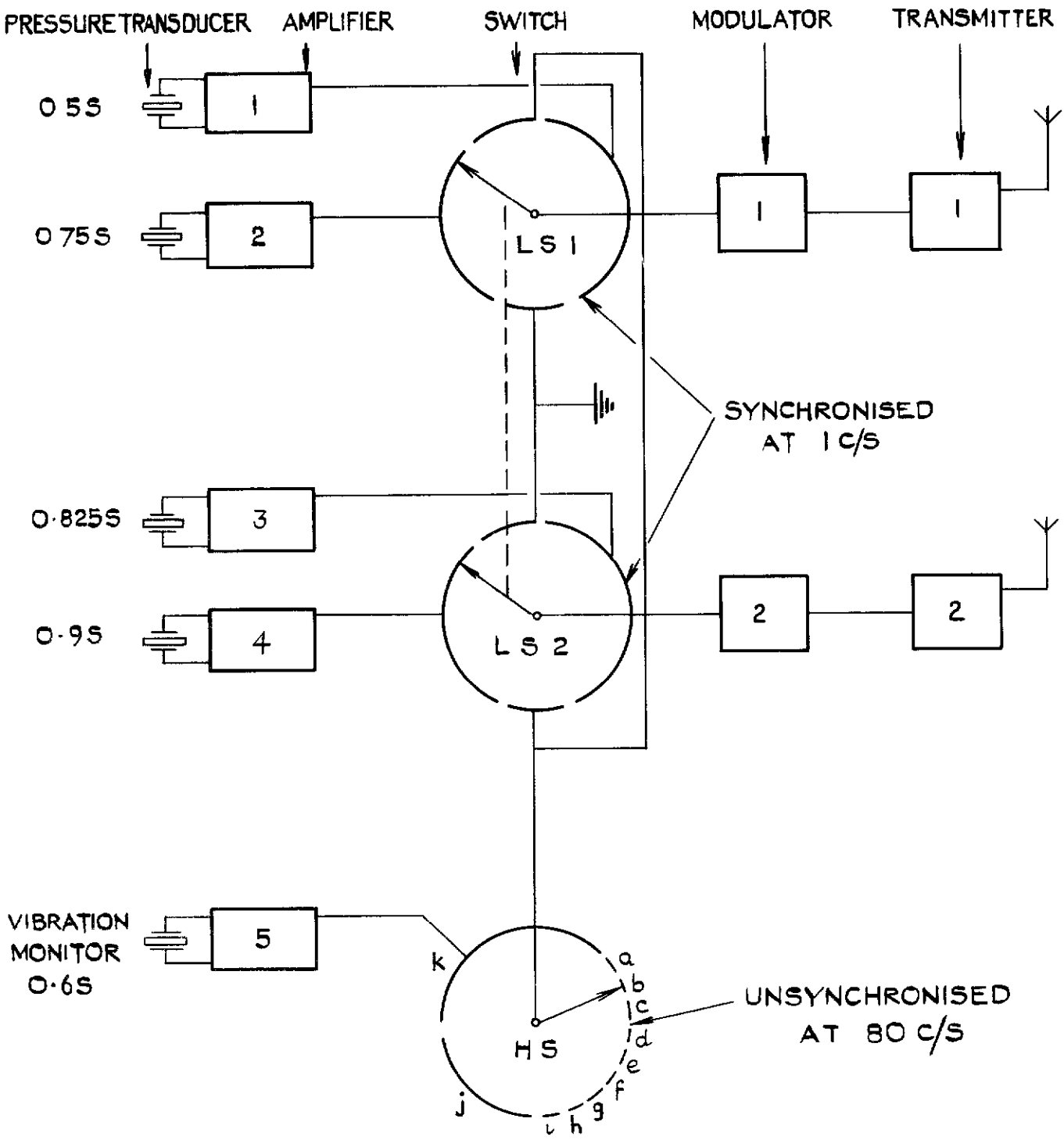

a	MARKER	g	STATIC PRES (·5S)
b	NORMAL AFT ACCN	h	PITOT PRES (·825S)
c	LATERAL C.G ACCN	ι	STATIC PRES (·825S)
d	LATERAL AFT ACCN	j	NORMAL CG ACCN
e	INCIDENCE	k	VIB^{N} MONITOR (·6S)
f	PITOT PRES (·5S)		

FIG. 19 TELEMETRY SWITCHING ARRANGEMENT FOR MODEL 3

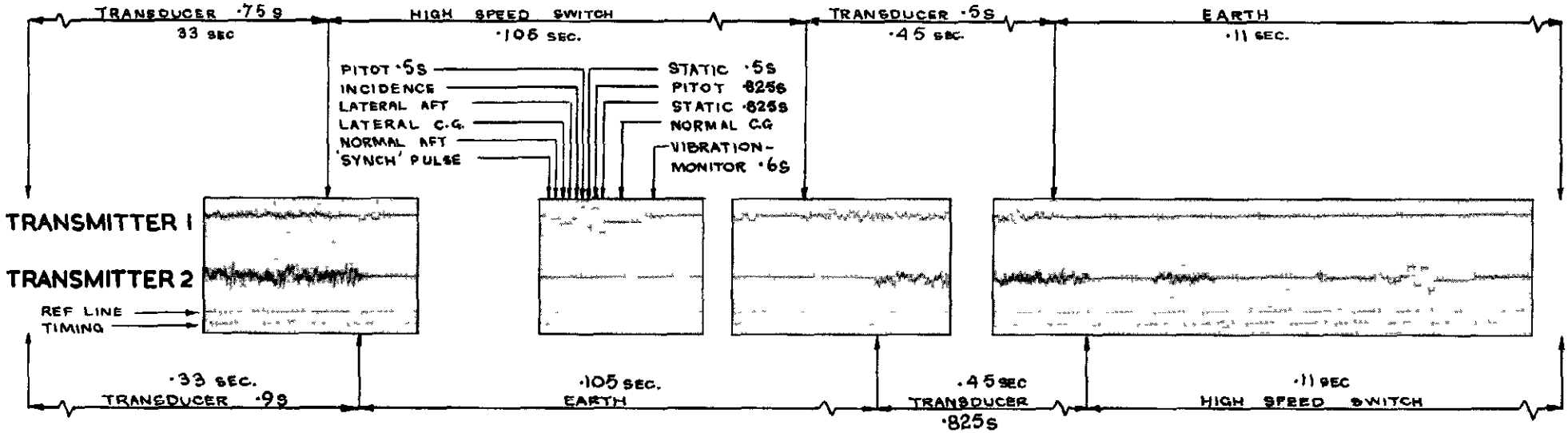

a Record at time 15.10 - 16 10 secs

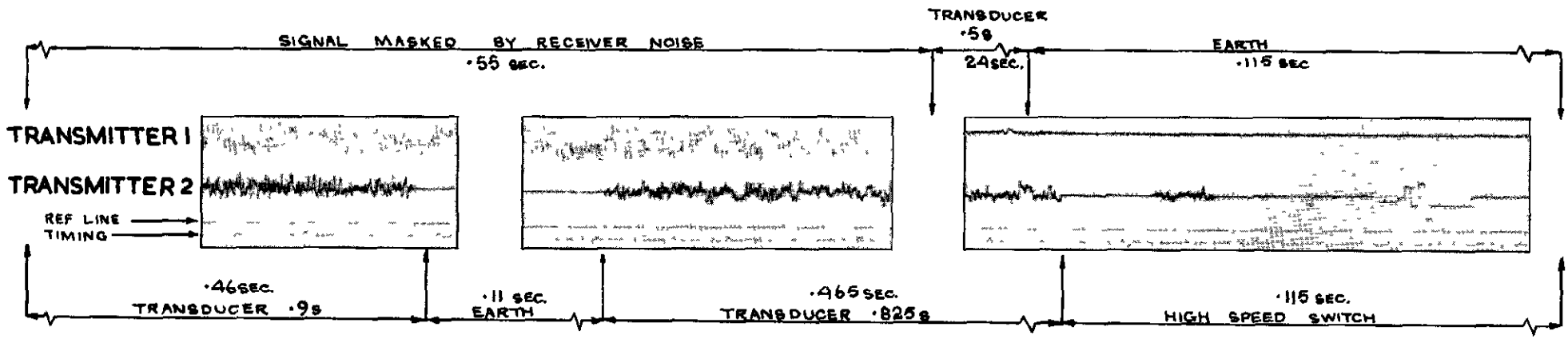

b Record at time 18.36 - 19 51 secs

Fig.20. Sample telemetry records for model 3

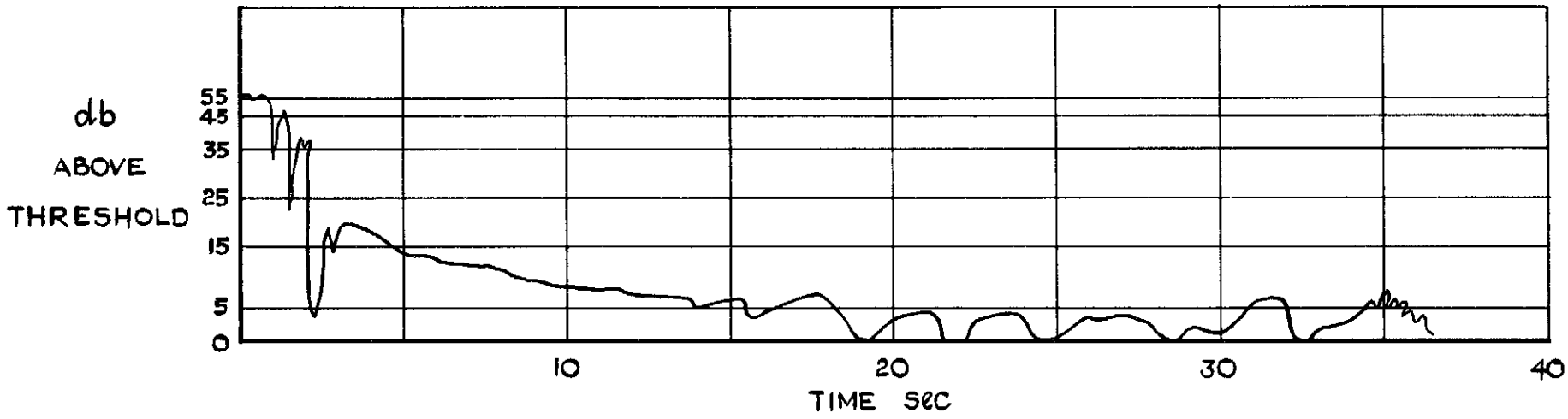

a TRANSMITTER 1 SIGNAL STRENGTH

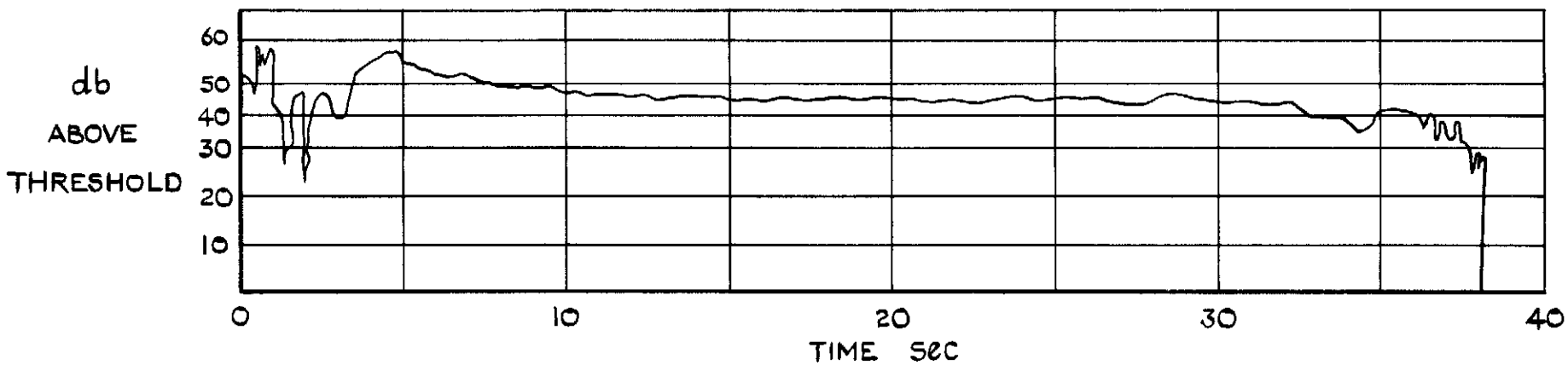

b TRANSMITTER 2 SIGNAL STRENGTH

FIG. 21 a & b R.F. SIGNAL STRENGTH RECORDS FOR MODEL 3

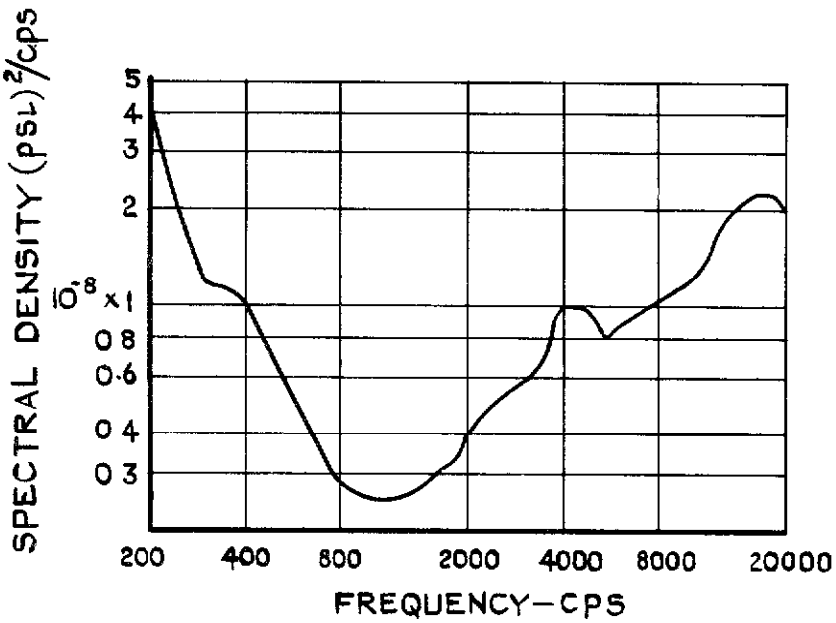

a TRANSMITTER 2, AT ZERO TIME

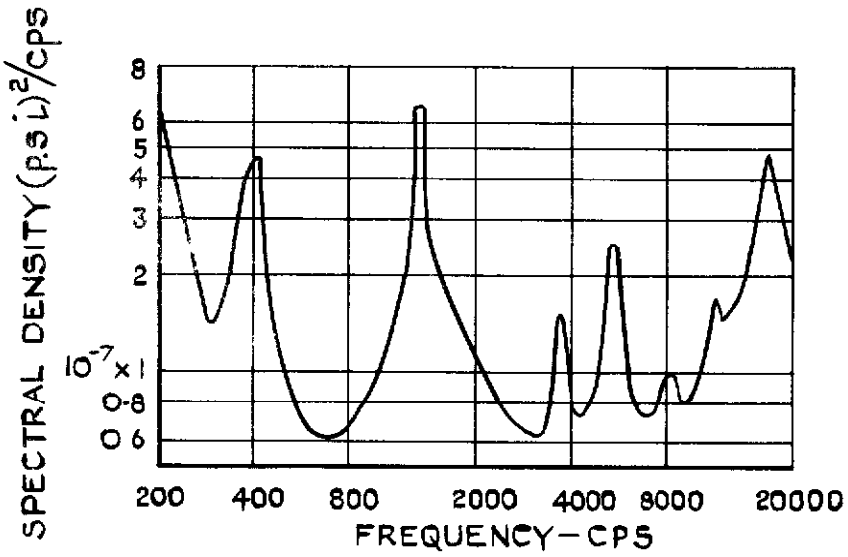

b TRANSMITTER 1, AT 20 TO 26 SECONDS

FIG. 22 a & b BACKGROUND NOISE SAMPLES (MODEL 3)

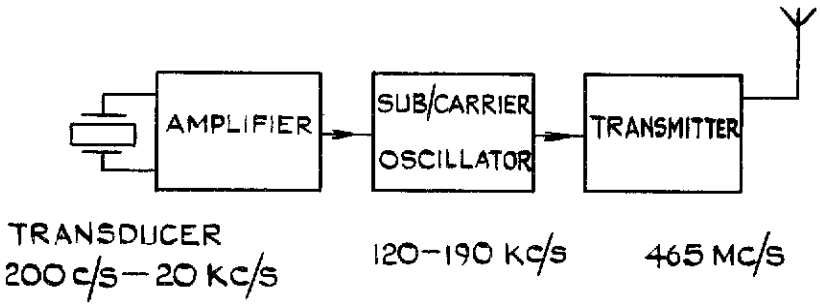

a AIRBORNE TELEMETRY SYSTEM

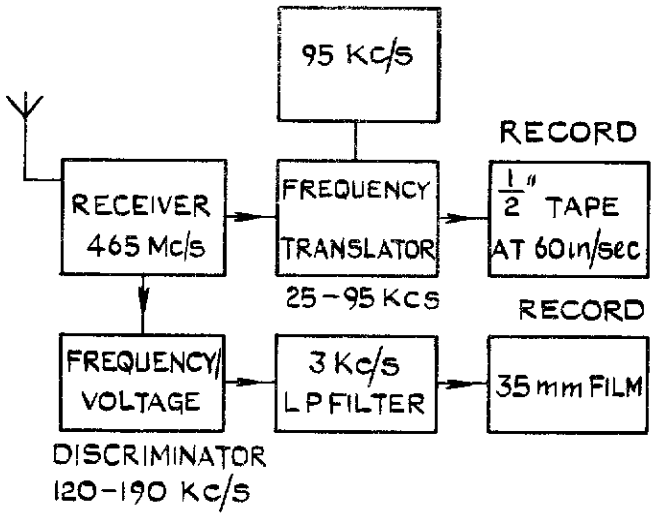

b GROUND RECEIVER AND RECORDING SYSTEM

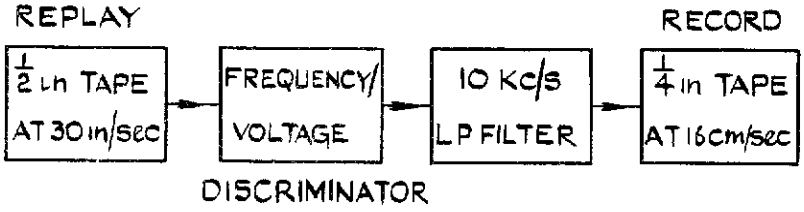

c TAPE RECORDING TRANSLATION

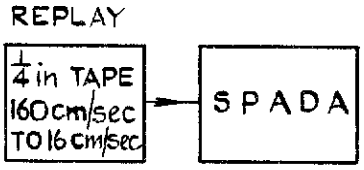

d ANALYSIS

FIG 23 DATA HANDLING PROCEDURE

Printed in England for Her Majesty's Stationery Office by the Royal Aircraft Establishment, Farnborough. Dd.129528. K.3.

A.R.C. C.P. No. 985 533.6.048.2 :
October 1966 531.787 :
532.526.7 :
Turner, K.J. 533.693.3 :
Walker, D. 533.6.011.35

MEASUREMENTS OF PRESSURE FLUCTUATIONS AND SKIN FRICTION ON THE UPPER SURFACE OF A SLENDER WING AT LIFT (M = 0.8 TO 2.0)

Four slender-wing free-flight models were used to investigate the local pressure fluctuations, skin-friction and static-pressures across one spanwise station under varying conditions of lift and Mach number. At Mach numbers between 0.8 and 1.2 a well-established free-vortex flow was achieved over the upper surface. The intention was to determine the ratio between the intensity of the pressure fluctuations and the local skin-friction under conditions of attached and separated flows.

(Over)

A.R.C. C.P. No. 985 533.6.048.2 :
October 1966 531.787 :
532.526.7 :
Turner, K.J. 533.693.3 :
Walker, D. 533.6.01135

MEASUREMENTS OF PRESSURE FLUCTUATIONS AND SKIN FRICTION ON THE UPPER SURFACE OF A SLENDER WING AT LIFT (M = 0.8 TO 2.0)

Four slender-wing free-flight models were used to investigate the local pressure fluctuations, skin-friction and static-pressures across one spanwise station under varying conditions of lift and Mach number. At Mach numbers between 0.8 and 1.2 a well-established free-vortex flow was achieved over the upper surface. The intention was to determine the ratio between the intensity of the pressure fluctuations and the local skin-friction under conditions of attached and separated flows.

(Over)

A.R.C. C.P. No. 985 533.6.048.2 :
October 1966 531.787 :
532.526.7 :
Turner, K.J. 533.693.3 :
Walker, D. 533.6.011.35

MEASUREMENTS OF PRESSURE FLUCTUATIONS AND SKIN FRICTION ON THE UPPER SURFACE OF A SLENDER WING AT LIFT (M = 0.8 TO 2.0)

Four slender-wing free-flight models were used to investigate the local pressure fluctuations, skin-friction and static-pressures across one spanwise station under varying conditions of lift and Mach number. At Mach numbers between 0.8 and 1.2 a well-established free-vortex flow was achieved over the upper surface. The intention was to determine the ratio between the intensity of the pressure fluctuations and the local skin-friction under conditions of attached and separated flows.

(Over)

DETACHABLE ABSTRACT CARDS

While measurements of reasonable quality were obtained, the inherent limitations of the telemetry system did not allow a sufficiently broad band of pressure-fluctuation frequencies to be measured so that the relationship with skin-friction could not be determined. Therefore, a detailed analysis of the results and comparison with other experimental or theoretical data has not been attempted. But the present results are considered to be a useful and significant addition to the rather meagre experimental data that exists on this subject, particularly because they were obtained in conditions free from flow imperfections such as free-stream turbulence which exist in most wind-tunnels.

While measurements of reasonable quality were obtained, the inherent limitations of the telemetry system did not allow a sufficiently broad band of pressure-fluctuation frequencies to be measured so that the relationship with skin-friction could not be determined. Therefore, a detailed analysis of the results and comparison with other experimental or theoretical data has not been attempted. But the present results are considered to be a useful and significant addition to the rather meagre experimental data that exists on this subject, particularly because they were obtained in conditions free from flow imperfections such as free-stream turbulence which exist in most wind-tunnels.

While measurements of reasonable quality were obtained, the inherent limitations of the telemetry system did not allow a sufficiently broad band of pressure-fluctuation frequencies to be measured so that the relationship with skin-friction could not be determined. Therefore, a detailed analysis of the results and comparison with other experimental or theoretical data has not been attempted. But the present results are considered to be a useful and significant addition to the rather meagre experimental data that exists on this subject, particularly because they were obtained in conditions free from flow imperfections such as free-stream turbulence which exist in most wind-tunnels.

Published by
HER MAJESTY'S STATIONERY OFFICE

To be purchased from
49 High Holborn, London W C.1
423 Oxford Street, London W.1
13A Castle Street, Edinburgh 2
109 St. Mary Street, Cardiff
Brazennose Street, Manchester 2
50 Fairfax Street, Bristol 1
258-259 Broad Street, Birmingham 1
7-11 Linenhall Street, Belfast 2
or through any bookseller

C.P. No. 985

S.O. CODE No. 23-9017-85